An-Najah National University

Faculty of Graduate Studies

ELECTRIC FIELD EFFECT IN MONOLAYER OF GRAPHENE

By

Salsabeel Khalel Saleh

Supervisor

Prof. Mohammed El-Said

This Thesis is Submitted in Partial Fulfillment of the Requirements for the Degree of Master of Physics, Faculty of Graduate Studies, An-Najah National University, Nablus, Palestine.

2022

ELECTRIC FIELD EFFECT IN MONOLAYER OF GRAPHENE

By

Salsabeel Khalel Saleh

This Thesis was Defended Successfully on 5/9/2022 and approved by

Prof. Mohammed El-Said Supervisor	M. Khalil Signature
Dr. Hussein Shanak External Examiner	 Signature
Prof. Mohammed S Abu- Jafar Internal Examiner	Mohd S. Signature

Dedication

Thanks, and praise to Allah who gave me life.

To the messenger of knowledge and holy religion – prophet Mohammed

For my father and my mother

For my husband and my daughter

For my family

To whom taught me the best way to increase my knowledge my dear teachers and lectures

Acknowledgements

I would like to thank my supervisor Prof. Mohammed Khalil El-Said, who encouraged me to complete this thesis. I also thank him for his efforts, time and guidance.

I do not forget the great thanks to Mr. Ayham Shaer for his efforts with us especially in Mathematica program.

Finally, my great gratitude to Physics Department at An-Najah National University

Declaration

I, the undersigned, declare that I submitted the thesis entitled:

ELECTRIC FIELD EFFECT IN MONOLAYER OF GRAPHENE

I declare that the work provided in this thesis, unless otherwise referenced, is the researcher's own work, and has not been submitted elsewhere for any other degree or qualification.

Student's Name: Salsabeel khaled Mahmoud Saleh

Signature: Salsabeel khaleel

Date: 5/9/2022

Table of Contents

List of Tables

List of Figures

Electric Field Effect in Monolayer of Graphene

By
Salsabeel Khalel Saleh
Supervisor
Prof. Mohammed El-Said

Abstract

Background: Graphene is a two-dimensional nanomaterial. The theory of graphene was laid out for the first time in 1947when P. R. Wallace looked at the electronic band structure of graphene. Many researchers have studied the properties of graphene in the presence of an electric field. This study has looked at the dynamics of electron in a two-dimensional monolayer graphene in the presence of a static and uniform electric field. Three different orientations of the electric field have been considered:
$\vec{E} = E_x\hat{\imath}$, $\vec{E} = E_y\hat{\jmath}$ and $\vec{E} = E_x\hat{\imath} + E_y\hat{\jmath}$ where x and y are arbitrary directions.

Methodology: The dynamical expressions for the velocity and position of an electron in an oriented- electric field have been derived from the dispersion relation. The figures in the calculations were drawn by using the Mathematica program.

Results: The electric field depended on the frequency of w_B.Because the electric field $\vec{E}$ is implicitly related to electron momentum $k_x$and k_y, it was possible control it as they change. Moreover, when the applied electric field $\vec{E}$ is in the x and y direction together the electron's behavior in the monolayer graphene is influenced by an angle α.

Conclusion: These findings showed that if an electric field $\vec{E}$ is applied to an electron along the x axis, the electron's Bloch oscillation would disappear in the x direction but would never happen in the y direction. And the electron's movement over the Dirac points would double the amplitude and period.

Keywords: Electric field; Bloch oscillation; graphene; position; velocity.

Chapter One

Introduction

Due to the development of atomic force microscope (AFM) and the scanning probe microscopy (SPM), particularly scanning tunneling microscope (STM) in 1980s nanotechnology and nanoscience progress took a curve up [1].

1.1 Nanomaterial

Nanoscience is the study of Nanomaterials which are materials with at least one dimension in nanoscale dimension (1-100 nm) or smaller. A nanometer is one-billionth of a meter or 10^{-9} m.

What makes nanomaterials really special is their unique properties, the properties of the nanomaterial are different from the bulk due to the high surface area over volume ratio as decreasing size. An increasingly larger percentage of atoms reside at its surface so there will be a high surface reactivity with the surrounding surface [1]. And the quantum size effect (QSE) changes the dependence of the density of state (DOS) on the energy for 3D, 2D, 1D, 0D [2] [3].

The properties of nanomaterials depend on the shape and size which influence the chemical, physical, electrical, optical and mechanical properties of a substance. Nanomaterials are classified according on their size (1- 100 nm) in at least one dimension and to their dimensionality [4].

For all solid-state system, the dimensionality refers to the number of degrees of freedom in the carrier's momentum. If the number of degrees of freedom is labeled as D_f and the number of directions of quantum confinement are labeled as Dc, then clearly [5]:

$$D_f + Dc = 3 \tag{1.1}$$

A quantum confined structure will be classified into three categories in the nanoscale as quantum wells (QWs), quantum well wires (QWWs) and quantum dot (QD).

The basic type of quantum confined structure is shown in Table 1.1 [4].

Table 1.1

Classification of quantum confined structures.

Structure	Number of free dimension (D_f)	Quantum confinement (Dc)
Bulk	3	0
Quantum well	2	1
Quantum well wire	1	2
Quantum dots	0	3

As more number of the dimension is confined, more discrete energy levels can be found, in other words, carrier movement is strongly confined in a given dimension.

Density of electron states in 3D, 2D, 1D and 0D semiconductor structure is shown in Figure 1.a.

Figure 1.A

Effect of quantum confinement on the density of electronic states [6]

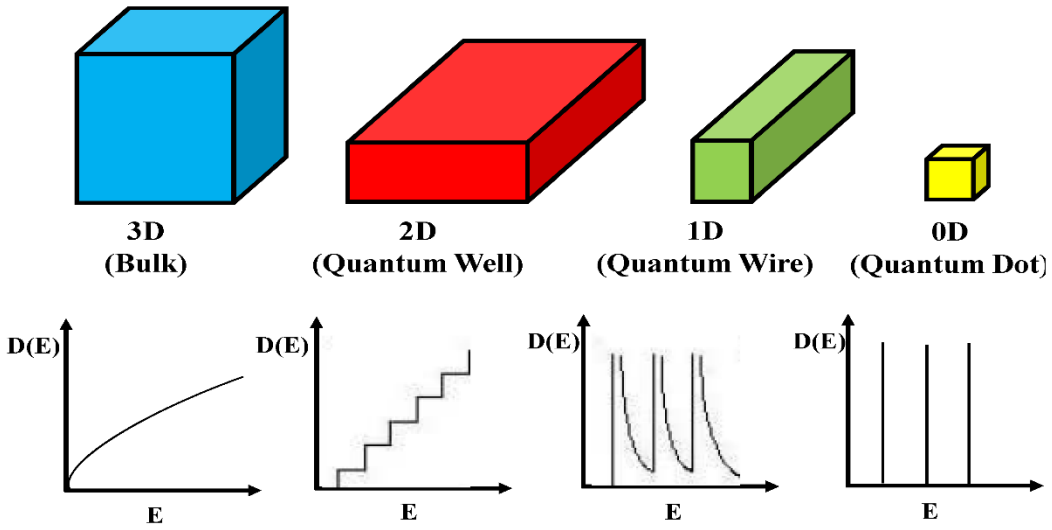

For these systems, the quantum size effect modifies the relationship between the density of states D(E) and energy E as follows:

Table 1.2

The relationship between the density of states D(E) and energy E.

Structure	relationship between the density of states D(E) and energy E
3D	$D(E) \sim \sqrt{E}$
2D	$D(E) \sim$constant
1D	$D(E) \sim \frac{1}{\sqrt{E}}$
0D	$D(E) \sim \sum_v \delta(E - E_v)$

In our study we want to focus on the exact 2D nanomaterial shells especially on the graphene.

1.2 Electronic structure of Graphene

The theory of graphene was developed when Wallace studied the electronic band structure of graphene in 1947 [7].

Graphene is a two-dimensional one atom thick planar sheet of bound carbon [8]. It's a single layer of three dimensional graphite which made of several layers of graphene sheets held together by Van der Walls forces. The differences in structure of graphene and graphite are shown in Figure 1.b.

Figure 1.B

A diagram of graphite (a) and graphene (b) [9] [10].

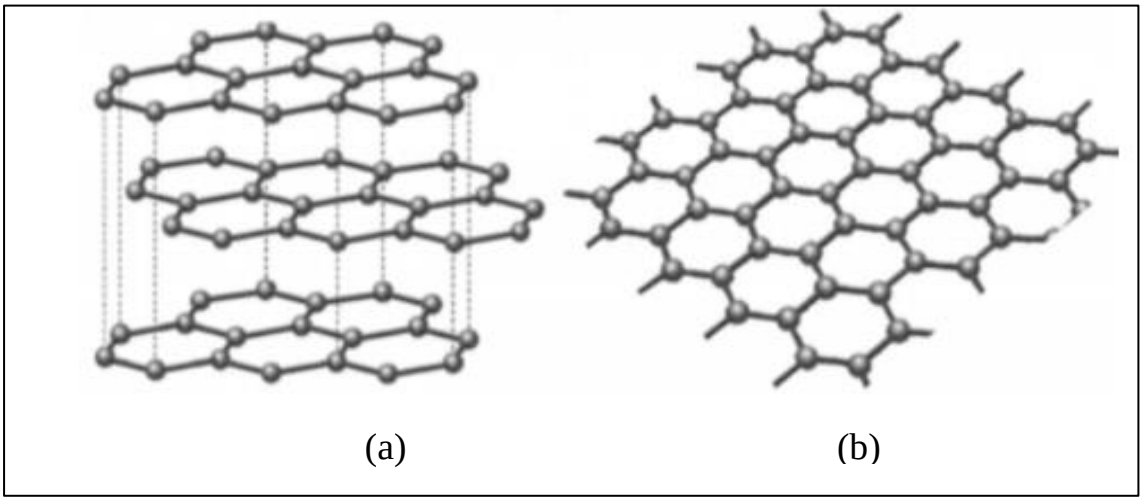

1.2.1 Crystal structure of graphene

In the carbon atom the atomic number is 6, so the electron configuration is $1s^2\ 2s^2\ 2p^2$. It has four valance electrons in the outer shell in the excited state. The arrangement of electrons and their relative spin in carbon atom is shown in Figure 1.c.

Figure 1.C

The arrangement of electrons and their relative spin in carbon atom [11].

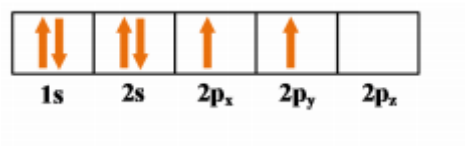

In graphene, the 2s, $2p_\chi$ and $2p_\gamma$ states interact covalently to form the three sp^2 hybrid orbitals. The arrangement of electrons and their relative spin in graphene is shown in Figure 1. d [12].

Figure 1.D

The arrangement of electrons and their relative spin in graphene [11].

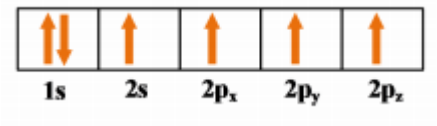

In graphene, the electrons in $2p_z$ orbitals participating in weaker π bonds. The electronic sp^2 hybrid states participate in three covalent σ bonds between each carbon and neighboring atom. An illustration of the different bonds of graphene is shown in Fig, 2.a [12]. An illustration of the sp^2 orbitals is shown in Figure 2.b [11].

Figure 2.A

An illustration of the different bonds of graphene.

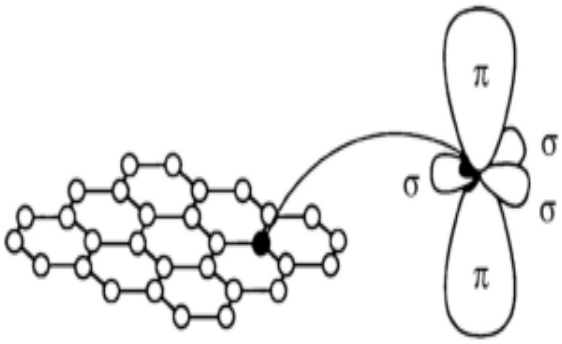

Figure 2.B

An illustration of the sp² orbitals.

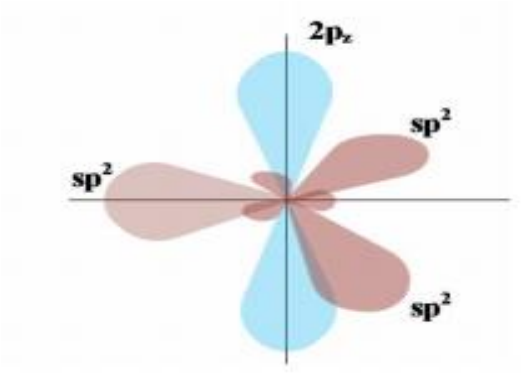

The π bond at the two inequivalent corners of the Brillouin zone form a Dirac points. The motion of the electrons in the graphene monolayer near the Dirac points $K\ and\ K'$ can be described by the massless Dirac Hamiltonian:

$$\hat{\mathrm{H}} = \hbar\, \upsilon_F \vec{\sigma}.\vec{P} \tag{1.2}$$

Where: υ_F is the Fermi velocity, σ the Pauli matrices and $\vec{P}$ is the electron momentum in two dimensions [13] [14].

The Pauli matrices $\sigma = (\sigma_x, \sigma_y)$ is a 2×2 Pauli matrices, where [12]:

$$\sigma_x = \begin{pmatrix} 0 & 1 \\ 1 & 0 \end{pmatrix} \tag{1.3}$$

And

$$\sigma_y = \begin{pmatrix} 0 & -i \\ i & 0 \end{pmatrix} \tag{1.4}$$

The graphene is a hexagonal lattice. In every unit cell there are two atoms. The unit cell defined by the unit vector $\vec{a}_1$ and $\vec{a}_2$ in the real space. Each two nearest neighbor atoms are separated by an interatomic distance a ≈ 1.42 Å. A hexagonal lattice with the lattice vectors is shown in Figure 2. c.

Figure 2.C

A hexagonal lattice with the lattice vectors [15].

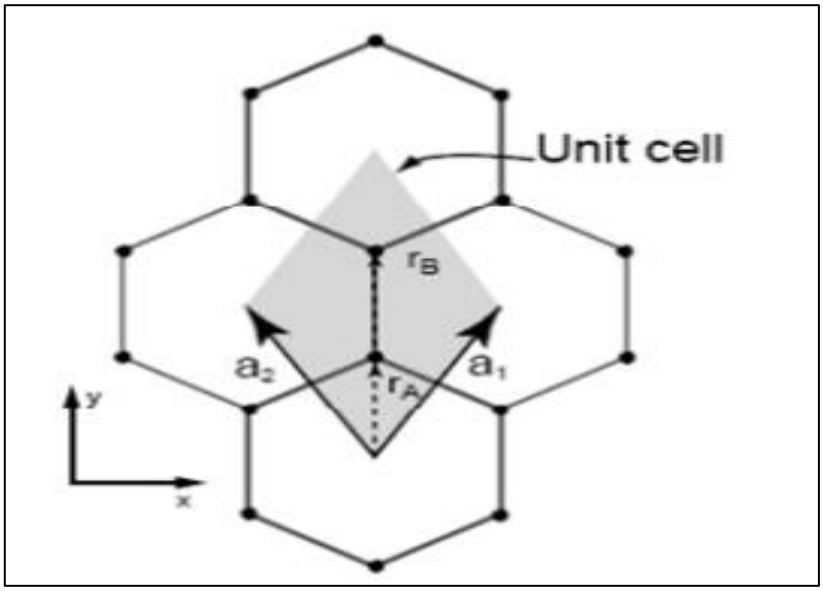

Each point on the periodic lattice can be described by $\vec{R} = m\vec{a}_1 + n\vec{a}_2$ [16].

The primitive lattice vector for the unit cell are given by:

$$\vec{a}_1 = \frac{\sqrt{3}a}{2}\left(\hat{e}_1 - \sqrt{3}\hat{e}_2\right) = \frac{a}{2}(\hat{e}_1 - \sqrt{3}\,\hat{e}_2) \tag{1.5}$$

and

$$\vec{a}_2 = \frac{\sqrt{3}a}{2}\left(\hat{e}_1 + \sqrt{3}\hat{e}_2\right) = \frac{a}{2}(\hat{e}_1 + \sqrt{3}\,\hat{e}_2) \tag{1.6}$$

Where the vectors ($\hat{e}_1$, $\hat{e}_2$, $\hat{e}_3$) are the orthonormal set.

The lattice constant $a = |\vec{a}_1| = |\vec{a}_2| = \sqrt{3}a \approx 2.46$ Å .

The primitive reciprocal lattice in the k space are given by [12]:

$$\vec{b}_1 = 2\pi\,\frac{\vec{a}_2 \times \hat{e}_3}{\vec{a}_1 \cdot (\vec{a}_2 \times \hat{e}_3)} = \frac{2\pi}{a}\left(\hat{e}_1 - \frac{\hat{e}_2}{\sqrt{3}}\right) \tag{1.7}$$

$$\vec{b}_2 = 2\pi\,\frac{\hat{e}_3 \times \vec{a}_1}{\vec{a}_1 \cdot (\vec{a}_2 \times \hat{e}_3)} = \frac{2\pi}{a}\left(\hat{e}_1 + \frac{\hat{e}_2}{\sqrt{3}}\right) \tag{1.8}$$

Figure 2.D

The reciprocal lattice point and the first Brillouin zone. The six corners of the first [15]. Brillouin zone K and K' are known as Dirac points [17]

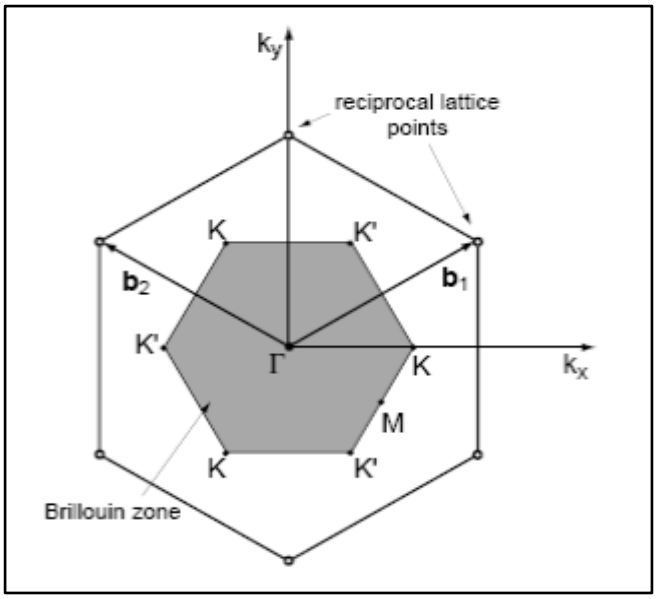

The first Brillouin zone for graphene in reciprocal space is seen in Figure 2.b. According to convention, the origin of the first Brillouin zone, which is designated as Γ where k = 0, corresponds to the center of the first Brillouin zone, where k = (k_x, k_y) is the wave vector linked to the electronic states in the lattice, with k_x and k_y standing for the wavenumbers along e1 and e2, respectively. Six K and K′ points, commonly known as Dirac points, make up the hexagonal initial Brillouin zone. A primitive reciprocal lattice vector divides points with the same label, which are regarded as equivalent ($b_1$or b_2).

1.2.2 The energy dispersion relation of graphene

The energy dispersion relation of the graphene $\epsilon^{(\pm)}(k)$ had been derived by using Tight binding method in [7]

$$\epsilon^{(\pm)}(k) = \frac{\in_0 \pm t\, f(k)}{1 \pm s\, f(k)} \tag{1.9}$$

Where $\epsilon = \epsilon^{(\pm)}(k)$ is the energy, s is an overlap parameter, t is a tight binding hopping parameter, + for the valence band and – for the conduction band, $\in_0$ is a parameter which set the zero of the dispersion relation, and $f(k)$ is a function defined by:

$$f(k) = \sqrt{1 + 4\cos\left(\frac{3k_y a}{2}\right)\cos\left(\frac{\sqrt{3}k_x a}{2}\right) + 4cos^2\left(\frac{\sqrt{3}k_x a}{2}\right)} \qquad (1.10)$$

Figure 3.A

A plot of the energy dispersion relation. The red is the conduction band and the blue is the valence band in the first Brillouin zone. The touch points between the conduction and valance bands are called the Dirac points (zero energy band gap) [12].

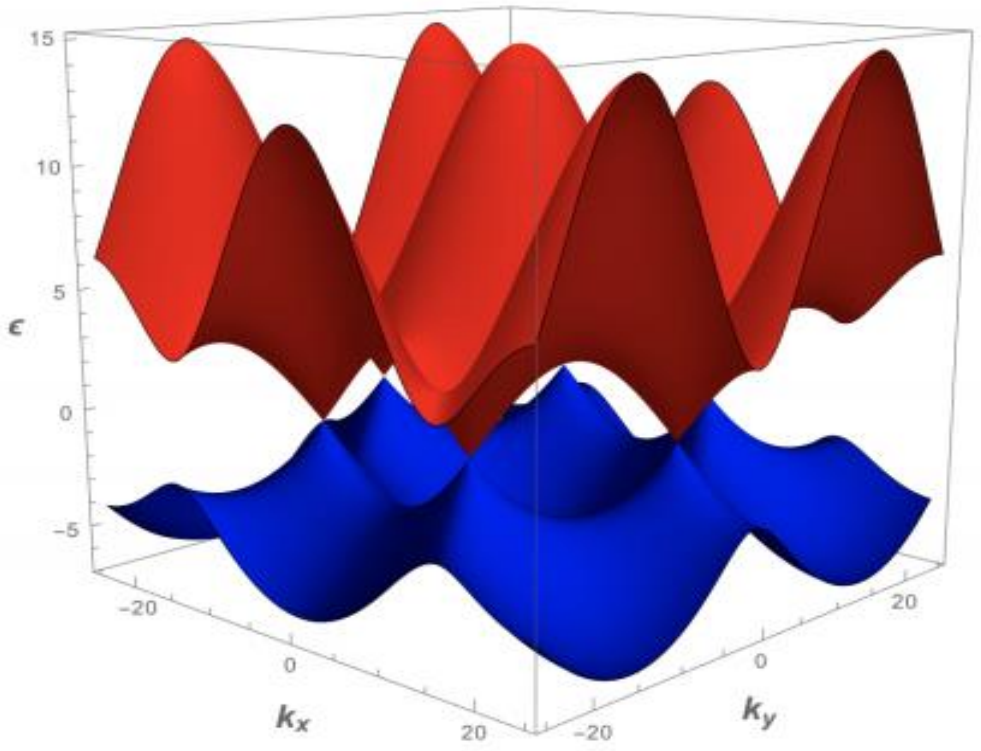

Figure 3.B

Conduction band and valence band in graphene touch each other at the Dirac points K and K′ [10].

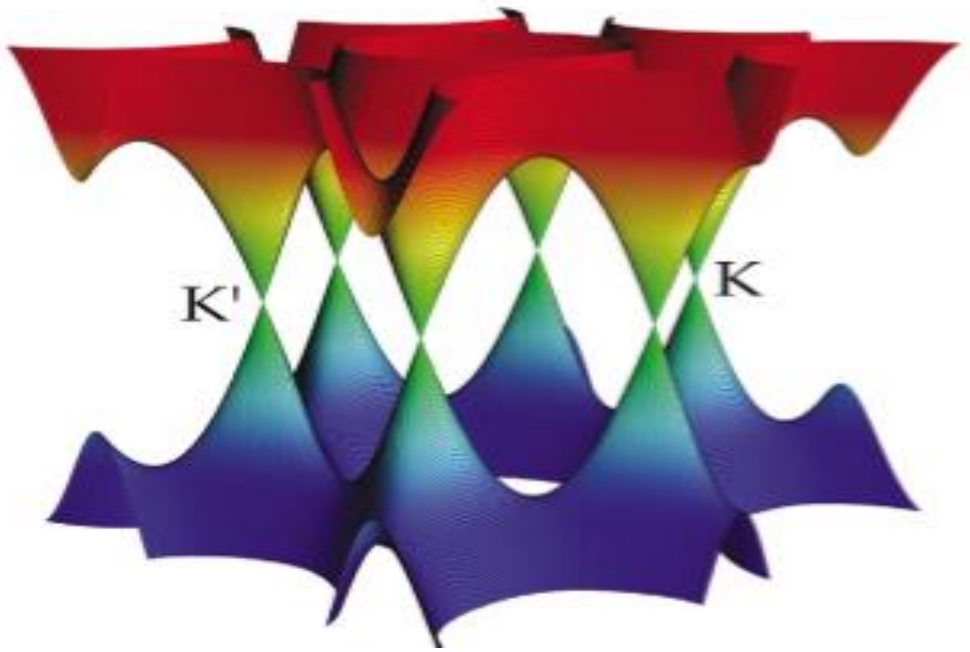

The graphene's valence and conduction bands overlap at six locations (the Dirac points of the reciprocal lattice), according to the band structure, implying a zero bandgap. Graphene therefore is semi-metallic. The zeros of the function f within the first Brillouin zone correspond to the six (Dirac) locations where the valence and conduction bands touch. The zeros are located at:

$$k \in \left\{\left(\pm\frac{4\pi}{3\sqrt{3}a}, -\frac{4\pi}{3a}\right), \left(\pm\frac{4\pi}{3\sqrt{3}a}, 0\right), \left(\pm\frac{4\pi}{3\sqrt{3}a}, \frac{4\pi}{3a}\right)\right\} \tag{1.11}$$

Where, at every value ofk_y, the signs + and separate K points from K′ points, making two neighboring points inequal. Regarding graphene's employment in field effect transistors, the zero bandgap material's properties have a variety of consequences. First order Taylor expansion of the function f described by Eq. (1.8) yields the linearized equation, which can be used to estimate the behavior of the dispersion relation Eq. (1.7) around the Dirac points:

$$\epsilon^{(\pm)}(k - k_0) = \pm\hbar v_f \|k - k_0\| \tag{1.12}$$

Where$\hbar$ denoted by where is the reduced Planck constant, k_0 is the wave vector at a Dirac point, and v_f is the electrons' Fermi velocity, provided by:

$$v_f = \frac{3a|t|}{2\hbar} \approx \frac{1}{300}c \tag{1.13}$$

where c is the speed of light in vacuum [12].

Derivation of the energy dispersion relation of graphene (eq. 1.9) is shown below:

For general values of n, defining H as the transfer integral matrix, S as the overlap integral matrix, and j as a column vector

$$H\,\psi_j = E_j S\,\psi_j \tag{1.14}$$

The energies E_j may be determined by solving the secular equation:

$$\det(H - E_j S) = 0 \tag{1.15}$$

Where:

$$H = \begin{pmatrix} H_{11} & H_{12} \\ H_{21} & H_{22} \end{pmatrix} \tag{1.16}$$

$$S = \begin{pmatrix} S_{11} & S_{12} \\ S_{21} & S_{22} \end{pmatrix} \tag{1.17}$$

$$\psi = \begin{pmatrix} C_{j1} \\ C_{j2} \end{pmatrix} \tag{1.18}$$

In the following, we will omit the subscript j = 1 in eq. (1.14) and eq. (1.15).

To monolayer graphene, the tight-binding model is used allows us to write the diagonal matrix element corresponding to the A sublattice as:

$$H_{AA} = \frac{1}{N}\sum_{i=1}^{N}\sum_{j=1}^{N} e^{ik.(R_{A.j} - R_{A.i})} \left\langle \emptyset_A(r - R_{A.i}) \middle| H \middle| \emptyset_A(r - R_{A.j}) \right\rangle \tag{1.19}$$

The previous equation includes a double summation over all the A sites of the lattice, if we assume that the dominant contribution arises from the same site j= i within every unit cell, then:

$$H_{AA} \approx \frac{1}{N}\sum_{i=1}^{N}\langle \emptyset_A(r - R_{A.i})\big|H\big|\emptyset_A(r - R_{A.j})\rangle \tag{1.20}$$

The summation's matrix member $\langle \emptyset_A|H|\emptyset_A\rangle$ has the same value on every A site, meaning it is unaffected by the site index i. We made it equal to the following parameter:

$$\in = \langle \emptyset_A(r - R_{A.i})\big|H\big|\emptyset_A(r - R_{A.j})\rangle \tag{1.21}$$

So,

$$H_{AA} \approx \frac{1}{N}\sum_{i=1}^{N} \in = \in \tag{1.22}$$

On average, they barely affect the electronic band structure. The carbon atoms on the two sublattices are chemically similar and have the same structure as those on the A sublattice. This indicates that the diagonal transfer integral matrix element for the B sublattice is equal to that for the A sublattice:

$$H_{BB} = H_{AA} = \in \tag{1.23}$$

Similar to how the transfer integral's diagonal elements are calculated, the overlap integral matrix's do the same. In this instance, a 2pz orbital on the same atom has an overlap that is equal to one.

$$\langle \emptyset_A(r - R_{A.i})\big|H\big|\emptyset_A(r - R_{A.j})\rangle = 1 \tag{1.24}$$

If the contribution from the same site dominates,

$$S_{AA} = \frac{1}{N}\sum_{i=1}^{N}\sum_{j=1}^{N} e^{ik.(R_{A.j}-R_{A.i})} \langle \emptyset_A(r-R_{A.i})|H|\emptyset_A(r-R_{A.j})\rangle$$

$$\approx \frac{1}{N}\sum_{i=1}^{N}\langle \emptyset_A(r-R_{A.i})|H|\emptyset_A(r-R_{A.j})\rangle$$

$$= \frac{1}{N}\sum_{i=1}^{N} 1 \quad = 1 \tag{1.25}$$

As the A sublattice and B sublattice share the same structure, once more:

$$S_{BB} = S_{AA} = 1 \tag{1.26}$$

The off-diagonal matrix element is:

$$H_{AB} = \frac{1}{N}\sum_{i=1}^{N}\sum_{j=1}^{N} e^{ik.(R_{B.j}-R_{A.i})} \langle \emptyset_A(r-R_{A.i})|H|\emptyset_B(r-R_{B.j})\rangle \tag{1.27}$$

There are three such neighbors for each A atom, hence it is possible to write the

contribution of the nearest neighbors to the off-diagonal matrix element as:

$$H_{AB} \approx \frac{1}{N}\sum_{i=1}^{N}\sum_{l=1}^{3} e^{ik.(R_{B.j}-R_{A.i})} \langle \emptyset_A(r-R_{A.i})|H|\emptyset_B(r-R_{B.j})\rangle \tag{1.28}$$

The matrix element between adjacent atoms$\langle \emptyset_A|H|\emptyset_B\rangle$, is independent of the indices I and l and has the same value for any pair of adjacent atoms. We made a parameter equal to it. It is customary to express t in terms of a positive parameter $\delta_0 = -t$ because t it is negative, where:

$$\delta_0 = -\langle \emptyset_A(r-R_{A.i})|H|\emptyset_B(r-R_{B.j})\rangle \tag{1.29}$$

Then we write the off-diagonal transfer integral matrix element as:

$$H_{AB} \approx -\frac{1}{N}\sum_{i=1}^{N}\sum_{l=1}^{3} e^{ik.(R_{B.j}-R_{A.i})} \quad \delta_0 \qquad = -\frac{\delta_0}{N}\sum_{i=1}^{N}\sum_{l=1}^{3} e^{ik.\delta_l}$$

$$= -\delta_0\, f(k) \tag{1.30}$$

The other off-diagonal matrix element H_{BA} is the complex conjugate of H_{AB}.

$$H_{AB} \approx -\delta_0\, f(k) \qquad and \qquad H_{BA} \approx -\delta_0 f^*(k)$$

A calculation of an off-diagonal element of the overlap integral matrix proceeds in a similar way as for the transfer integral, so:

$$S_{AB} = S_0 f(k) \qquad and \qquad S_{BA} = S^* = S_0 f^*(k)$$

Summarizing the results:

$$H_1 = \begin{pmatrix} \in & -\delta_0\, f(k) \\ -\delta_0 f^*(k) & \in \end{pmatrix} \tag{1.31}$$

$$S_1 = \begin{pmatrix} 1 & S_0 f(k) \\ S_0 f^*(k) & 1 \end{pmatrix} \tag{1.32}$$

where we emphasize that these matrices apply to monolayer graphene by using the subscript "1" By resolving the secular equation $\det(H - E_j S) = 0$, the corresponding energy E can be found.

$$det\begin{pmatrix} \in -E & -(\delta_0 + E) f(k) \\ -(\delta_0 + E) f^*(k) & \in -E \end{pmatrix} = 0 \tag{1.33}$$

$$(E-\in)^2 - ([E-\in]S_0 + \in\ S_0 + \delta_0)^2\ |f(k)|^2 = 0 \tag{1.34}$$

Solving this quadratic equation yields the energy:

$$\epsilon^{(\pm)}(k) = \frac{\in_0 \pm \delta_0\, f(k)}{1 \pm s\, f(k)} \tag{1.35}$$

1.2.3 Density of states for the 2D materials and Graphene:

The dispersion relation of the 2D nanomaterials like graphene at Dirac points K and K′, can be obtained as:

$$\in (\vec{k}) = \hbar\, v_f |\vec{k}| = \hbar\, v_f \sqrt{k_x^2 + k_y^2} \tag{1.36}$$

By using the common definition of the density of state, $D(E) = \sum \delta(\epsilon - \epsilon(\vec{k}))$, the DOS for the graphene can be given as [18]:

$$D(E) = \frac{2|E|}{\pi\hbar^2 v_f^2} \tag{1.37}$$

1.2.4 Properties of Graphene:

The graphene nanomaterial has the following attractive properties:

- Optical Properties:
  Graphene has a large range capability to absorb the light from the infrared to the ultraviolet.

- Electronic Properties:
  Graphene is called a zero gap because the conduction and valance band touch each other at the Dirac points.

- Mechanical Strength:

  Graphene is one of the strongest materials due to the high strength of the carbon–carbon bond [19]. It can retain to its original dimension after applied strain so its elasticity [20].

- The material is chemically stable.
- Has high thermal conductivity.
- Has ballistic transport over submicron scale.
- It has large theoretical specific surface area ($2630\ m^2 g^{-1}$).
- High transmissivity of graphene ~ 98 % [31].

1.2.5 Fabrication of Graphene*:*

Graphene production was obtained on micromechanical exfoliation of graphite by using scotch- tape- method. In order to remove just one layer of graphene, this technique requires sticking an adhesive tape to graphite and pulling it away [21].

Micromechanical cleavage: crystallographers and crystal growers have used micromechanical cleavage. Researchers started producing multilayer films of graphene

from graphite as early as 1999 by performing a certain kind of micromechanical cleavage on the material. Since, micromechanical cleavage has been improved and can now create layers of high quality, with the size of the layers being constrained by the original graphite sample's single-crystal grains. Micromechanical cleavage is the preferred technique when conducting fundamental research on graphene in tiny batches.

Separating the layers from the bulk highly ordered pyrolytic graphite (HOPG) surface is the fundamental concept of mechanical cleavage. The highly ordered pyrolytic (HOPG) surface is covered with Scotch tape, which is then very gently peeled off to carry out the Scotch tape dry exfoliation procedure. After many pulls, the graphite layer gets thinner, and eventually, there is only one layer of graphene left

This approach offers large-area graphene flakes with excellent quality and all the desirable properties that make graphene such a promising material for several applications.

Anodic bonding: the microelectronics industry uses anodic bonding to attach silicon wafers to glass in order to shield them from contamination and humidity. Graphite is pushed onto a glass substrate and a high voltage is placed between the graphite and metal back contact to perform anodic bonding to create graphene. The glass substrate is then heated.

A few layers of graphite adhere to the glass during anodic bonding via electrostatic contact and are then able to be peeled away from the glass. The temperature and applied voltage are two factors that are utilized to regulate the number of layers. According to reports, anodic bonding results in graphene flakes that are around a millimeter wide.

Laser ablation and photo-exfoliation: It is still early in the development of laser ablation as a procedure to exfoliate graphene and requires more research. Laser ablation employs a laser beam to remove material from a solid surface. When irradiation results in the whole or partial separation of a layer, this is referred to as photo-exfoliation.

In laser ablation, graphite flakes are abated and exfoliated using laser pulses to create graphene. The number of layers of graphene created can be determined by adjusting the laser energy. Although laser ablation has been successfully used in liquids, it functions

best in an inert or vacuum environment. The graphene layers may oxidize as a result of laser ablation carried out in air.

Bottom-up graphene: the substrate is transition metal or silicon. The Chemical Vapor Deposition (CVD) chamber is vacuumed and heated in the presence of catalyst and hydrocarbon gases are induced and decomposed so deposits a spread of carbon atoms onto the surface of the substrate, thus forming the graphene layers.

Top-down graphene: is a process of exfoliation of graphite to produce a sheet of graphene [22].

Figure 3.C

All carbon forms [21].

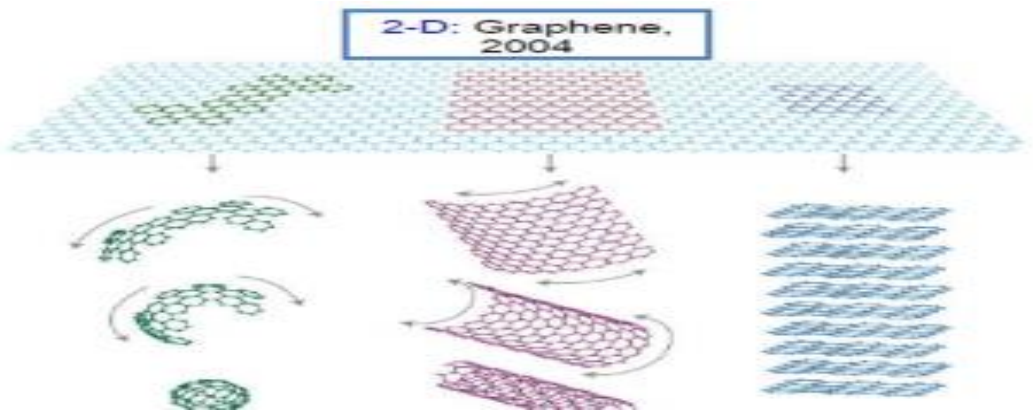

1.3 Applications of Graphene

1.3.1 Monolayer Graphene Field Effect Transistors (FET):

Two families can be used to categorize graphene FETs. Graphene is used as a current-carrying FET channel in the first class of graphene FET devices. Typically, this class of graphene FETs is used in:

1- back-gated.
2- top-gated.
3- dual-gated.

All these configurations are shown in Figure 3.d.

Figure 3.D

Illustrations of the cross sections of (a) a bottom-gated graphene FET, (b) a dual-gated graphene FET, and (c) A top-gated graphene FET.

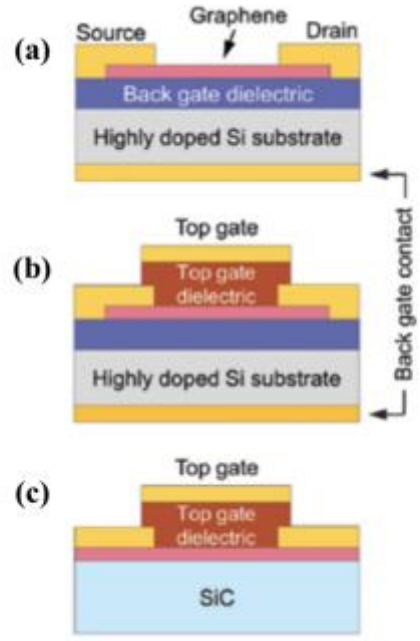

Graphene is employed to create the current-carrying channel between the source and the drain in each of these combinations. Utilizing a highly doped Si substrate, back-gated and dual gated graphene FET topologies are available. In dual-gated graphene FETs, a dielectric layer is deposited on top of the graphene channel, forming a top gate in addition to the back gate. In rear-gated graphene FETs, the substrate serves as the FETs back gate. Graphene is grown epitaxially on a SiC substrate for top-gated graphene FETs, and a top gate is created by depositing a dielectric on top of the graphene channel.HfO_2, SiO_2, and Al_2O_3 are a few of the dielectrics that are employed.

In 2007 Monolayer Graphene Field Effect Transistors (FET)was studied and demonstrated by Lemme et al. FET can be used in high frequency electronics knowing that the speed of FET in high frequency applications relays on the carrier mobility in the FET channel. In high frequency applications, a FET's speed is actually inversely correlated with the carrier mobility of the FET channel. Despite monolayer graphene's great mobility, the substrates and dielectric utilized cause it to lose mobility. A cross sectional diagram of a monolayer graphene FET is shown in Figure 3.e.

Figure 3.E

A cross sectional diagram of a monolayer graphene FET [12].

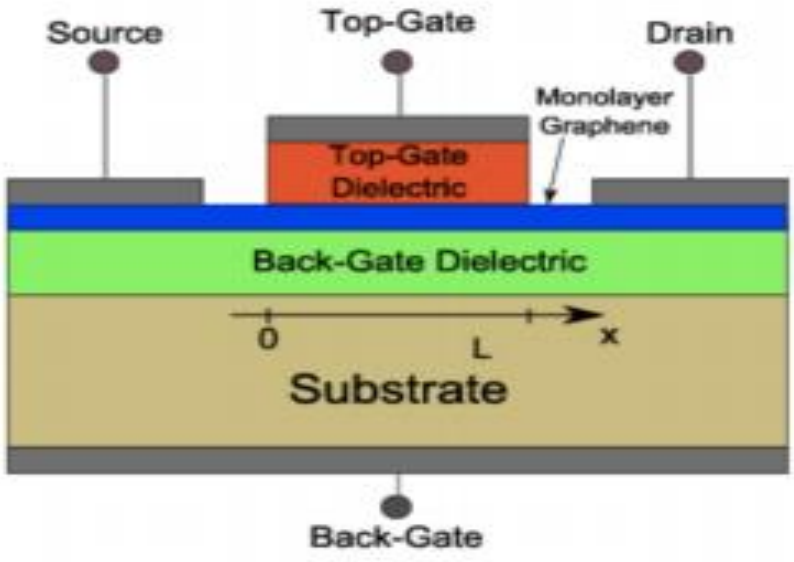

1.3.2 spintronics:

The aim is to utilize the spin degree of freedom in order to replace charge as the information carrier to achieve high speed, low power computing. The emerging material for spintronics was established to be graphene due to its gate tenability, low spin orbit coupling strength, negligible hyperfine interaction and high electronic charge mobility [13].

Spintronics in 2D semiconductor materials like black phosphorus and TMDCs can provide functionalities like gate-controlled amplification/switching operations that are not feasible when utilizing only graphene. In order to do this, Avsar et al. (2017a) showed that all electrical spin injection, transport, manipulation, and detection are possible at room temperature in ultrathin BP-based spin valves. Spin relaxation periods of up to 4.5 ns and spin relaxation lengths of more than 6 m were derived using measurements of the four-terminal Hanle spin precession as shown in fig.4.a.

Elliott-Yafet relaxation is predominate in BP, as evidenced by temperature and gate voltage dependences for spin and momentum relaxation periods and strong agreement with first-principles predictions.

The majority of the early research into magnetism in 2D materials concentrated on proximity-induced and defect-induced magnetism. Indeed, intrinsic ferromagnetic order is not anticipated in 2D single layers according to the Mermin-Wagner theorem. The experimental findings from 2D $Cr_2Ge_2Te_6$, where magnetism is absent in its monolayer at least down to the lowest observed temperatures (4.7 K), initially provided support for this. The critical temperature in this material lowers considerably from 68 K (bulk) to 30 K (bilayer), which can be explained by the thermal excitation of spin waves, yet ferromagnetic order still remains down to the bilayer level.

Figure 4.A

Spintronics in 2D Materials Beyond Graphene

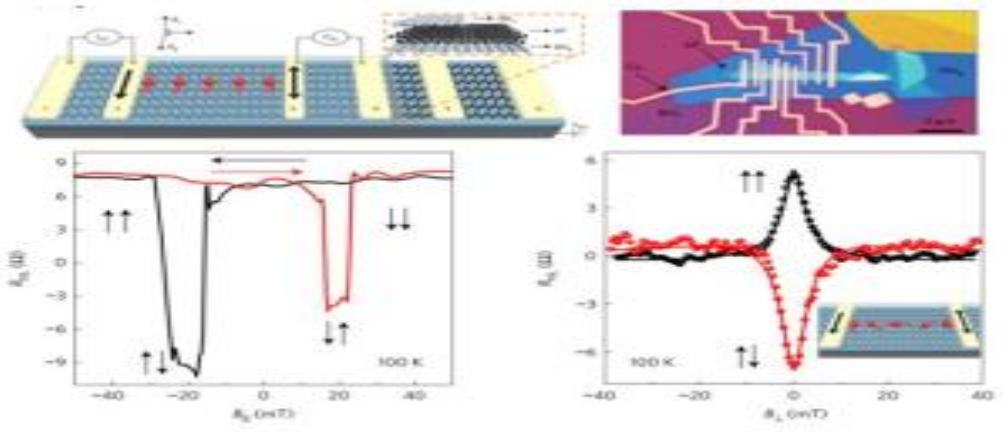

1.3.3 Medical Applications:

Effective uses of graphene in biomedicine were created, the movement of DNA via membranes made of graphene nanopores.

The devices were made of nanopores that were shaped by electron beams and had a thickness of 1 to 5 nm in graphene. The authors noticed greater blocked currents for graphene nanopores than for conventional solid-state nanopores because of the thinness of the membranes. In contrast to silicon nitride nanopores, ionic current noise levels were several orders of magnitude higher. The device's 5 nm of $TiO_2$was deposited in atomic layers to eliminate these variations. Graphene is a superior electrical conductor, in contrast to conventional solid-state nanopore materials, which are insulating.

In another work on DNA translocation through graphene medical applications that nanopores nanosized holes that can transport ions and molecules-are very promising devices for genomic screening, in particular DNA sequencing.

By covering a micro size hole in a silicon nitride membrane with a graphene flake and using an electron beam to drill a nanosized hole in the graphene, the pores were created. Future single-molecule genomic screening devices will be possible thanks to the characteristic transient conductance changes that were seen as individual DNA molecules translocated through the hole [23].

1.3.4 Energy storage

For the development of energy storage devices, graphene is perfect. The interconnected layers of graphene are highly conductive, which adds to the reasons for their attractiveness as applications in energy storage. Graphitic carbon is used to make anodic materials that are perfect for lithium ion batteries. Between two sheets of storage, where the Li and Carbon are located, there occurs an electron transfer. The energy capacity as a result is $372\ mA\ Hg^{-}$. Large diffusion distances are produced by the long-range crystal organization found in graphitic materials. Several studies have been undertaken in the last few decades to increase the specific energy capacity. An area that is less explored in the graphene realm, but has produced some interesting findings, is increasing the capacity of data storage devices while keeping the size of a (flash-drive scale) piece of hardware.

Indium tin oxide electrodes coated with polymers and graphene oxide have been demonstrated to have storing properties by researchers looking into graphene oxides. In the following years, graphene oxide-based devices with data capacity of 0.2 Tbits cm^3have been developed. This is roughly ten times as much storage as currently available 16 GB USB flash drives. In theory, graphene could replace current solid-state technologies in the future due to the increasing demand for more data storage if research is focused on increasing storage capacity. We contend that since USB flash drives are currently rather small, shrinking the size of devices is not as big of a problem. However, it would not be long until a terabyte could be stored on a device the size of a USB flash drive, all while keeping the price of the device as low as possible [24].

1.3.5 LCD smart windows and OLED displays

A layer of liquid crystals is sandwiched between two flexible electrodes made of a flexible polymer and graphene as part of the technology used in this device. The clear background with a decal placed in the center is revealed when the light-scattering liquid crystals are aligned by the electric field. The use of graphene as a flexible OLED counter electrode is the subject of extensive study into organic light emitting diode (OLED) displays.

Indium tin oxide counter electrodes, which are used in current OLED technology, are fragile and difficult to find globally. On the other hand, graphene ought to be practically unlimited and flexible. These gadgets are thought to be the ones where graphene makes its commercial debut due to reported interest from large corporations like Samsung. For mobile and tablet devices, flexible touch displays are among the applications of this technology. Perhaps curved screens for mobile phones won't be too far off with further development in this field! Even flexible three-dimensional displays are possible, which was unimaginable ten years ago.

Figure 4.B

Diagram showing the creation and creation of an LCD Smart Window (a-d), as well as a real LCD Smart Window in use (e) [24].

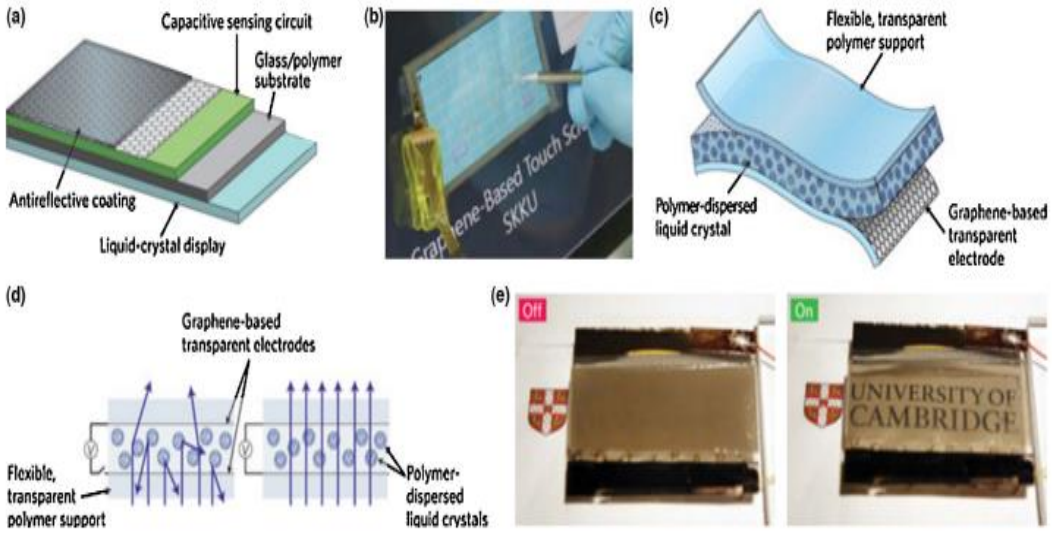

1.3.6 Solar cells

Another potential use for graphene is in photovoltaic or solar cells. The availability of platinum on earth would seem to be insufficient to produce a planet's worth of solar cells, which is related to the second disadvantage - the cost - of current solar cell technologies, which use platinum-based electrodes. Given that graphene is an excellent conductor, it may be possible to construct graphene electrodes that are lighter and less expensive while still being effective, as explained by Wang et al. Their graphene electrode demonstrated an efficiency of 7.8% in a dye-sensitized solar cell, 0.2% less than a counter electrode made of platinum but generated for a fraction of the price.

Obviously, it would be ideal to increase efficiency, but with modern technology, cost-cutting is just as big of a problem. However, any contribution to green energy will definitely be embraced by governments, activist groups, and homeowners who believe their power costs are too high [23].

1.3.7 Valley-Polarized Jets in Graphene

The electrons in ordinary materials and graphene. There are two possible momentum states for 2D materials or to store and process information within these valley states, researchers are interested in managing them. The creation of valley-polarized currents is a challenge in reaching that goal. Carolin Gold is now from the Zurich-based Swiss Federal Institute of Technology (ETH) and her coworkers have discovered a method to isolate an electron pair. jets in a bilayer sheet of graphene, one for each valley. The approach might be used in "valleytronic" someday. Equipment to separate electrons according to their valley state.

Graphene's valley states are typically identical, but under specific conditions, the electronic band structure can become asymmetric, or "trigonally distorted," giving rise to distinct momentum profiles for each valley. Theorists expected that this warping would result in numerous valley-polarized jets moving along a single graphene sheet in various directions. But it has proven challenging to isolate these jets.

Bilayer graphene was the material that Gold and her coworkers employed, and they hypothesized that it would also support valley-polarized jets. They positioned two metallic gates on top of the bilayer, spaced apart by a 50 nm-wide channel. The current

passing through the aperture was measured when the bilayer was subjected to a voltage. Using a metallic tip that causes an interference signal in the current measurements, they traced the course of this current.

Figure 4.C

Valley-Polarized Jets [41]

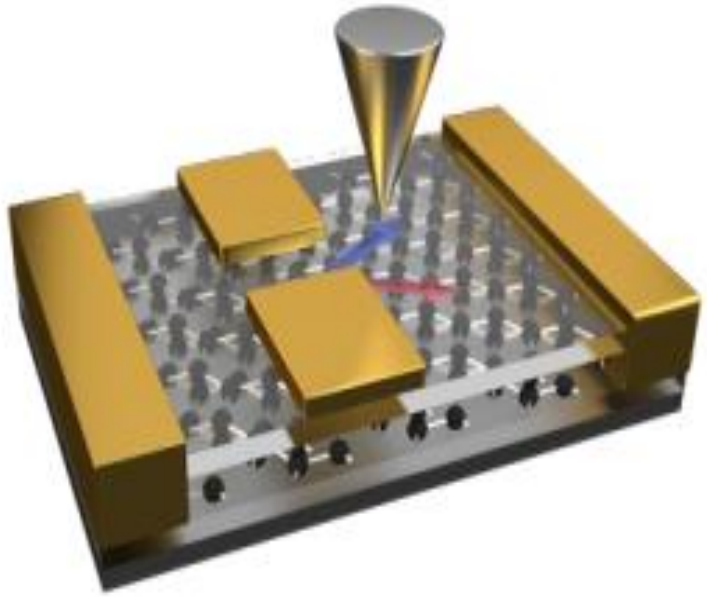

1.4 Literature survey

Different researchers had studied the properties of graphene in the presence of the electric field starting with:

- Novoselov et al. (2004). Studied the f electric fields in the graphene layers and discussed the use of graphene as channel material for FETs [25].
- Lukose, V., Shankar, R., & Baskaran, G. (2007). Studied the Landau levels in graphene in the presence of crossed uniform electric and magnetic fields [26].
- Liao and Duan. (2010). Studied the graphene as an emerging electronic material for future electronics due to its exceptionally high carrier mobility and single-atomic thickness [27]
- Miyazaki, H., Tsukagoshi, K., Kanda, A., Otani, M., & Okada, S. (2010). Studied the resistance, temperature of the conductance and mobility gap in bilayer graphene placed under a perpendicular electric field [28].

- Kumar, S. B., & Guo, J. (2011). Studied the electronic properties, effective mass, electron velocity, density-of-state and transformation of the band structure of multilayer graphene's in the presence of vert
- Orozco, F. A. S., Ochoa, J. G. A., Rivas, X. C., Figueroa, J. L. C., & Carrada, H. M. M. (2019). Studied the analytical energy eigenvalues of the graphene quantum dot interacting in the presence of AB-flux field and external magnetic field [30].

Elsaid et al have worked on the magnetic and thermal properties of various nanomaterials:

- Tiryaki, A. A. S. (2013). Studied the electronic band structure of graphene and carbon nanotube [31].
- Shaer, A. A. (2015). Studied the heat capacity of two electrons confined in a quantum dot present in an external magnetic field [32].
- Hijaz, MY. E (2016). Studied the magnetization of two interacting electrons confined in doubled quantum dot under the effect of an applied uniform magnetic field [33].
- Bzour, F. M. (2016). Studied the effects of the hydrostatic pressure and temperature on the properties of the (GaAs) single quantum dot in a magnetic field [34].
- Ali, M. M. M. (2017). Studied the magnetization of single electron in GaAs confined in a quantum dot presented in a magnetic field by solving the Hamiltonian [35]
- Elsaid,K.M Eshtiaq, Hijaz.E. (2017). Studied the magnetic susceptibility of coupled double GaAs quantum dot in magnetic fields [36].
- Ayham Shaer.A, Elsaid.K.M, Hijaz.A. (2019). Studied the heat capacity of a semiconductor quantum dot in magnetic fields [37].
- Elsaid.K.M, Shaer.A, Hjaz.E, Hajj Yahya.M. (2020). Studied the Impurity effect on the magnetization and magnetic susceptibility of an electron confined in a quantum ring under the presence of an external magnetic field [38].

1.5 Research Objectives

The main goal of this research project is to study the dynamics: (acceleration, velocity and position) of the electron inside a monolayer of graphene under the effect of an external electric field $\vec{E}$. Different directions of the electric field will be considered as:

Case 1: $\vec{E}$ along the x direction.

Case 2: $\vec{E}$ along the y direction.

Case 3: $\vec{E}$ along the arbitrary direction.

Chapter Two

Theory

This chapter explains the mobility of an electron in pristine monolayer graphene subjected to a constant external electric field using the dispersion relation obtained be the TBM (tight binding method).

2.1 Dispersion relation of energy

A monolayer of graphene subjected to a constant electric field will be studied, and the dynamics of the electron will be investigated based on the dispersion relation $\varepsilon\,(k)$ derived by the tight binding assumption.

We first use dispersion relations to get the formula for electron motion, and then we look at the features of the Bloch oscillation. The honeycomb structure of monolayer graphene is well known, and its dispersion relation can be stated as:

$$\mathcal{E}(k) = \pm\varepsilon\sqrt{3 + f(k)} \tag{2.1}$$

Where the sign (+) refers to the electron in the conduction band, while the sign (-) refers to the hole in the valance band. ε refers to the Fermi velocity, ε ≈ 2.5 eV,

$$f(k) = 4\cos\left(\frac{3}{2}ak_x\right)\cos\left(\frac{\sqrt{3}}{2}ak_y\right) + 2\cos\left(\sqrt{3}ak_y\right) \tag{2.2}$$

a≈1.42 Å refers to the carbon- carbon distance.

At Dirac points (DPs) the electron energy band and the hole energy band come together [39].

Figure 4.D

The energy dispersion relation of a Dirac points at graphene. Left plot in the absence of the electric field and the right in the presence of an applied perpendicular electric field (applied $\vec{E} \rightarrow E_g$*) [12].*

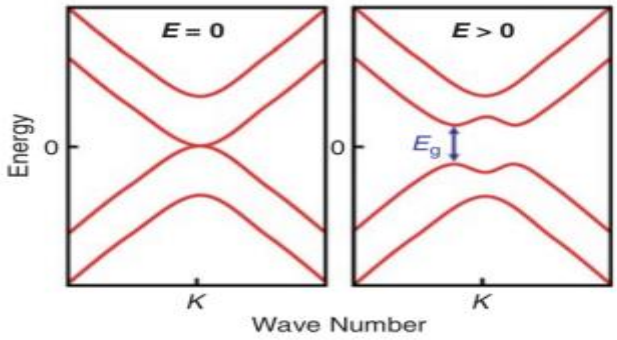

From Eq. (2.1) and the condition $\varepsilon\,(k) = 0$ the DPs are placed at $\left[\frac{4n\pi}{3a}, \frac{2}{\sqrt{3}a}\left(2n \pm \frac{2}{3}\right)\pi\right], \left[\frac{2}{3a}(2n+1)\pi, \frac{2}{\sqrt{3}a}\left(2n \pm \frac{1}{3}\right)\pi\right]$ with $n = 0 \pm 1, \pm 2, \ldots$. [39]

2.2 Bloch Oscillation

Bloch oscillations are caused by the coherent motion of quantum particles in periodic configurations in solid-state physics. It explains how the electron will oscillate when a constant force is exerted on it.

The velocity of the carriers (electrons and holes) will be computed by using the relations:

$$\upsilon = \frac{1}{\hbar}\frac{\partial \varepsilon(\mathrm{k})}{\partial \mathrm{k}}, \upsilon = (v_x, v_y) \tag{2.3}$$

As a function of k_x and k_y, we can easily obtain $\upsilon = (v_x, v_y)$ [23]

$$v_x = \pm \frac{3a\varepsilon \cos\left(\frac{\sqrt{3}}{2}k_y a\right)\sin\left(\frac{3}{2}k_x a\right)}{\hbar\sqrt{f(k)+3}} \tag{2.4}$$

$$v_y = \pm \frac{\sqrt{3}a\varepsilon\,[\cos\left(\frac{3}{2}k_x a\right)\sin\left(\frac{\sqrt{3}}{2}k_y a\right) + \sin(\sqrt{3}\,k_y a)]}{\hbar\sqrt{f(k)+3}} \tag{2.5}$$

The velocities of electrons (hole or electron) are denoted by the sign "-" and "+".

The velocity of the massless Dirac electrons when a constant electric field $E = (E_x, E_y)$ was pinned to the Fermi velocity and the electric field moved the Dirac points around the momentum space.

D'ora et al. show that when a constant electric field is applied along a graphene layer, massless Dirac electrons' velocity is pinned to the Fermi velocity in a finite field, and the electric field moves the Dirac point around in momentum space. Dirac electrons in the electric field can be viewed as crucial particles since their motion is a drift transport, which means they move ballistically and leave footprints [39]. As a result, when there is an electric field present, the wave packet's momentum follows:

$$-\hbar\frac{d\vec{k}}{dt} = \vec{F}_{ext} = -qE \tag{2.6}$$

For example consider 1D system's using tight binding approximation the dispersion relation is given as,

$$\varepsilon_n(k) = \varepsilon_0 - t_0 2\cos(ka) \tag{2.7}$$

We use the relation $v = \frac{dr}{dt}$, then we get:

$$k(t) - k(0) = -\frac{qtE}{\hbar} \tag{2.8}$$

When $k(0) = 0$, $k = k(t) = -\frac{qtE}{\hbar}$.

From Eq. (2.2), $v = \frac{1}{\hbar}\frac{\partial \mathcal{E}(\mathrm{k})}{\partial \mathrm{k}} = \frac{2at_0}{\hbar}\sin(ka) = -\frac{2at_0}{\hbar}\sin\left(\frac{qatE}{\hbar}\right)$

Afterward, the electron's position oscillates in space and time as:

$$x = \frac{2\ t_0}{qE}\cos\left(\frac{qatE}{\hbar}\right) \tag{2.9}$$

With time, the location x oscillates.

$$\omega_B = \frac{aqE}{\hbar} \tag{2.10}$$

One Bloch oscillation's period needs to be less than the relaxation time at room temperature, which is $\tau = 10^{-14}$s, in order to be observed [40].

For 2D case as in graphene monolayer with x and y components as:

$$k_x(t) = k_x(0) - \frac{qE_x}{\hbar}t \qquad (2.8\ a)$$

$$k_y(t) = k_y(0) - \frac{qE_y}{\hbar}t \qquad (2.8\ b)$$

Where $k_x(0)$, $k_y(0)$ are the initial wave vector value.

2.3 The dynamics of the electron in the presence of $\vec{E}$

In this part we want to present the dynamics (acceleration, velocity and position) of the electron inside a monolayer of graphene under the effect of an external electric field $\vec{E}$:

Case 1: $\vec{E}$ along the x direction.

Case 2: $\vec{E}$ along the y direction.

Case 3: $\vec{E}$ along the arbitrary direction.

2.3.1 Case 1: $\vec{E}$ is along x- axis $\vec{E} = E\hat{\imath}$

$\vec{E}$ is taken to be along the x direction. Because $E_y = 0$ in this situation, we obtain $k_y(t) = k_y = constant$, and $k_x(t) = k_x(0) - \frac{qE_x}{\hbar}t$. Assuming $k_x(0) = 0$, the v_x and v_y dynamic formula are:

$$v_x(t) = \pm\frac{3a\varepsilon\cos\left(\frac{\sqrt{3}}{2}k_y a\right)\sin\left(-\frac{2\pi}{T}t\right)}{\hbar\ \mathrm{G(t)}} \qquad (2.11)$$

$$v_y = \pm\frac{\sqrt{3}a\varepsilon\ [\cos\left(-\frac{2\pi}{T}t\right)\sin\left(\frac{\sqrt{3}}{2}k_y a\right) + \sin(\sqrt{3}\,k_y a)]}{\hbar\ \mathrm{G(t)}} \qquad (2.12)$$

Where $G(t) = \sqrt{4\cos\left(\frac{\sqrt{3}}{2}k_y a\right)\cos\left(-\frac{2\pi}{T}t\right) + 3 + 2\cos\left(\sqrt{3}\,k_y a\right)}$ .And T is the period of motion $T = \frac{4\pi}{3}\,\frac{\hbar}{|qaE_x|}$. It's simple to observe that $v(t+T) = v(t)$.

The Bloch oscillation's frequency and circular frequency are commonly provided by:

$$v_B = \frac{1}{T} \quad and \quad \omega_B = 2\pi v_B \tag{2.13}$$

For the electron the time dependent position r(t) according to the formulation of v is $\vec{r}(t) = \vec{r}(0) + \int_0^t \vec{v}\,dt$ we assume here the initial position $r(0) = 0$. i.e. $x(0) = 0$ and $y(0) = 0$.

We get the following result via a simple derivation:

$$x(t) = C - \frac{\varepsilon}{qE_x}G(t) \tag{2.14}$$

where C is an integration constant that satisfies $x(0) = 0$. We must numerically calculate the following for y(t)

$$y(t) = -\frac{2\,\omega_B\,\varepsilon}{\sqrt{3}\,qE_x}\int_0^t \frac{\cos(-\omega_B t)\sin\left(\frac{\sqrt{3}}{2}k_y a\right) + \sin\left(\sqrt{3}k_y a\right)}{G(t)}\,dt \tag{2.15}$$

2.3.2 Case 2: $\vec{E}$ is along y- axis $\vec{E} = E\hat{j}$

$\vec{E}$ along the y direction. Because $E_x = 0$ in this situation, we obtain $k_x(t) = k_x = constant$, and $k_y(t) = k_y(0) - \frac{qE_y}{\hbar}t$. Assuming $k_y(0) = 0$, the v_x and v_y dynamic formula are:

$$v_x(t) = \pm\frac{3a\varepsilon\cos\left(-\frac{2\pi}{T'}t\right)\sin\left(\frac{3}{2}k_x a\right)}{\hbar\,G'(t)} \tag{2.16}$$

$$v_y(t) = \pm\frac{\sqrt{3}a\varepsilon\,[\cos\left(\frac{3}{2}k_x a\right)\sin\left(-\frac{2\pi}{T'}t\right) + \sin\left(-\frac{2\pi}{T'}t\right)}{\hbar\,G'(t)} \tag{2.17}$$

Where $G'(t) = \sqrt{4\cos\left(-\frac{2\pi}{T'}t\right)\cos\left(\frac{3}{2}k_x a\right) + 3 + 2\cos\left(-\frac{4\pi}{T'}t\right)}$. And T' is the period of motion $T' = \frac{4\pi}{3}\frac{\hbar}{|qaE_x|}$. It's simple to observe that $v(t+T') = v(t)$.

The Bloch oscillation's frequency and circular frequency are commonly provided by:

$$v'_B = \frac{1}{T'} \quad and \quad \omega_B = 2\pi v_B$$

Case 2 is similar to Case 1, $y(t) = C' - \frac{\varepsilon}{qE_x}G'(t)$, where C' is an integration constant that satisfies $y(0) = 0$. We must numerically calculate the following for x(t).

$$x(t) = -\frac{2\sqrt{3}\,\omega'_B\varepsilon}{q\,E_y}\int_0^t \frac{\cos(-\omega'_B t)\sin\left(\frac{3}{2}k_x a\right)}{G'(t)}\,dt \qquad (2.18)$$

2.3.3 Case 3: $\vec{E}$ is along x and y axis

$\vec{E}$ along the arbitrary direction in the plane of graphene monolayer. Because $E_x$and $E_y$have a value the electron dynamics became more complex. The initial phases $k_x(0)$ and$k_y(0)$, as well as the $\frac{E_x}{E_y}$ are also related to the parameters of $v_x(t)$and $v_y(t)$.

The function of $v_x$and $v_y$are periodic and both of them depends on cos ($\frac{3}{2}a\left|k_x(0) - \frac{qE_x}{\hbar}t\right|$) and cos ($\frac{\sqrt{3}}{2}a\left|k_y(0) - \frac{qE_y}{\hbar}t\right|$).

Let $T_x$and $T_y$identify the periods before and after hence, we have $T_x = \frac{4\pi}{3}\frac{\hbar}{|qaE_x|}$ and $T_y = \frac{4\pi}{\sqrt{3}}\frac{\hbar}{|qaE_y|}$ .Suppose $\frac{T_x}{T_y}$ is rotational, i.e $\frac{T_x}{T_y} = \frac{n}{m}$ where n and m are integers.

Chapter Three

Results and Discussion

In this chapter we will investigate the dynamics of the electron in a monolayer of graphene under the effect of the orientation of the electric field.

This chapter contains:

1. The dynamics of the electron when $\vec{E}$ along the x direction.
2. The dynamics of the electron when $\vec{E}$ along the y direction.
3. The dynamics of the electron when $\vec{E}$ along the arbitrary direction.

3.1 The dynamics of the electron when $\vec{E}$ along the x direction

In this part we went to study the dynamics of the electron in a monolayer of graphene.

Based on Eq. (2.14), we can find the maximum and minimum values for the position in the x direction:

$$x_{max} = C - \frac{\varepsilon}{|qE_x|}\sqrt{2\cos\left(\sqrt{3}ak_y\right) + 3 - 4\left|\cos\left(\frac{\sqrt{3}}{2}ak_y\right)\right|} \tag{3.1}$$

$$x_{min} = C - \frac{\varepsilon}{|qE_x|}\sqrt{2\cos\left(\sqrt{3}ak_y\right) + 3 + 4\left|\cos\left(\frac{\sqrt{3}}{2}ak_y\right)\right|} \tag{3.2}$$

So, along the x direction the oscillation amplitude L_x is:

$$L_x = |x_{max} - x_{min}|$$

$$= \frac{\varepsilon}{|qE_x|}\left|\left|2\cos\left(\frac{\sqrt{3}}{2}ak_y\right) + 1\right| - \left|1 - 2\cos\left(\frac{\sqrt{3}}{2}ak_y\right)\right|\right| \tag{3.3}$$

We calculate the maximum and minimum values for the amplitude L_x .

If we suppose that the inner of the cosine has a relation with n (where n is an integer number), It becomes $\frac{\sqrt{3}}{2}ak_y = (n+\frac{1}{2})\pi$. Suppose n=0, then $\frac{\sqrt{3}}{2}ak_y = \frac{\pi}{2}$, Put it in Eq. (3.3) of L_x ,then we get that $L_x^{min} = 0$.

According to the same Eq. (3.3) when $\left|\cos\left(\frac{\sqrt{3}}{2}ak_y\right)\right| \geq \frac{1}{2}$ we get the maximum value for the amplitude $L_x^{max} \approx 1084\ nm$ with $v_B \approx 237\ GHz$.

We went to study some variables by changing the value of k_y. We have displayed the dynamical variables and positions against $\omega_x t$ for selected values of k_y value. Then draw a graph to show the dynamics for the electron.

3.1.1 The velocity v_x along the x-axis:

Figure 5.a shows the dependence of x-component of electron velocity $v_x(t)$ against $\frac{t\omega_B}{\pi}$ for the case $k_y \to \frac{\sqrt{3}}{2}ak_y = 0$.

Figure 5.A

The velocity of the electron $\frac{v_x\, a\varepsilon}{\hbar}$ *against* $\frac{t\omega_B}{\pi}$ *when* $\frac{\sqrt{3}}{2}ak_y = 0$.

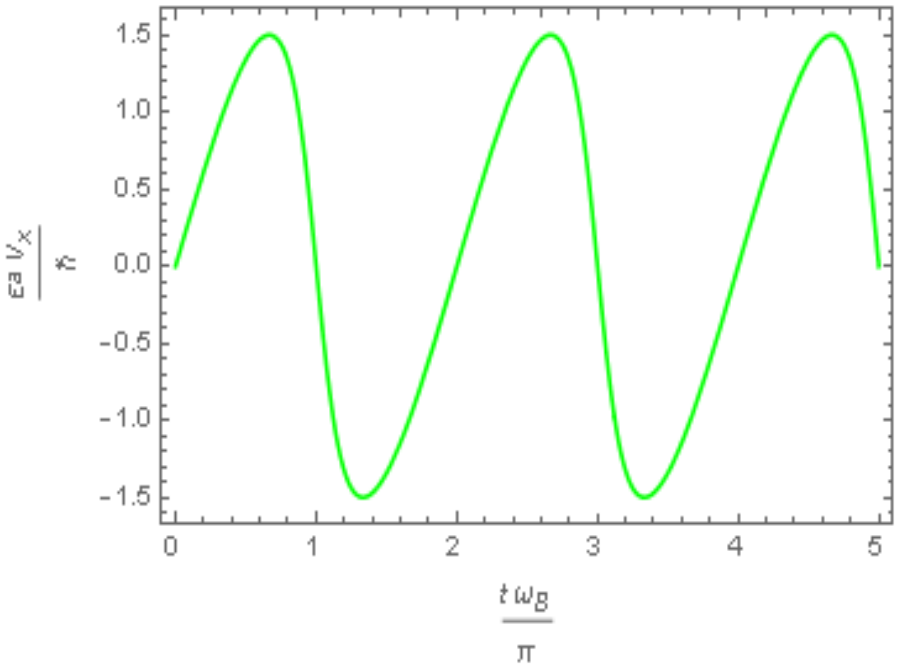

Figure 5.b shows the effect of the electric field in the x-direction $E_x$against the velocity of the electron v_xWhen $\frac{\sqrt{3}}{2}ak_y = \frac{\pi}{2}$. There is no oscillation through the x direction. Because $\frac{\sqrt{3}}{2}ak_y = \left(n + \frac{1}{2}\right)\pi$ so the cosine function vanishes.

Figure 5.B

The x-component of the velocity of the electron $\frac{\boldsymbol{v_x\, a\varepsilon}}{\hbar}$ *against* $\frac{\boldsymbol{t\omega_B}}{\boldsymbol{\pi}}$ *when* $\frac{\sqrt{3}}{2}\boldsymbol{ak_y} = \frac{\boldsymbol{\pi}}{\boldsymbol{2}}$.

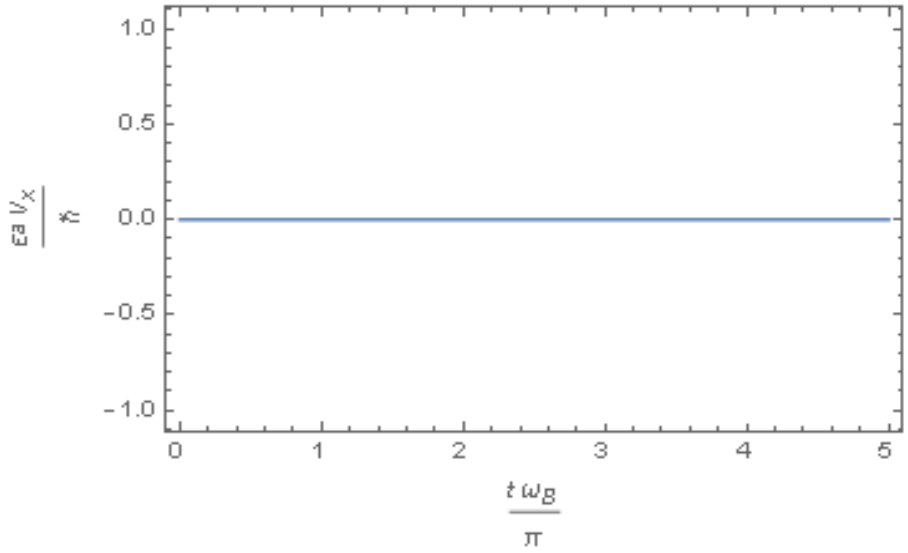

Figure 5.c shows the effect of the electric field in the x-direction $E_x$against the velocity of the electron v_xWhen $\frac{\sqrt{3}}{2}ak_y = \frac{5}{12}\pi$.

Figure 5.C

The velocity of the electron $\frac{\boldsymbol{v_x\, a\varepsilon}}{\hbar}$ *verses* $\frac{\boldsymbol{t\omega_B}}{\boldsymbol{\pi}}$ *when* $\frac{\sqrt{3}}{2}\boldsymbol{ak_y} = \frac{\boldsymbol{5}}{\boldsymbol{12}}\boldsymbol{\pi}$.

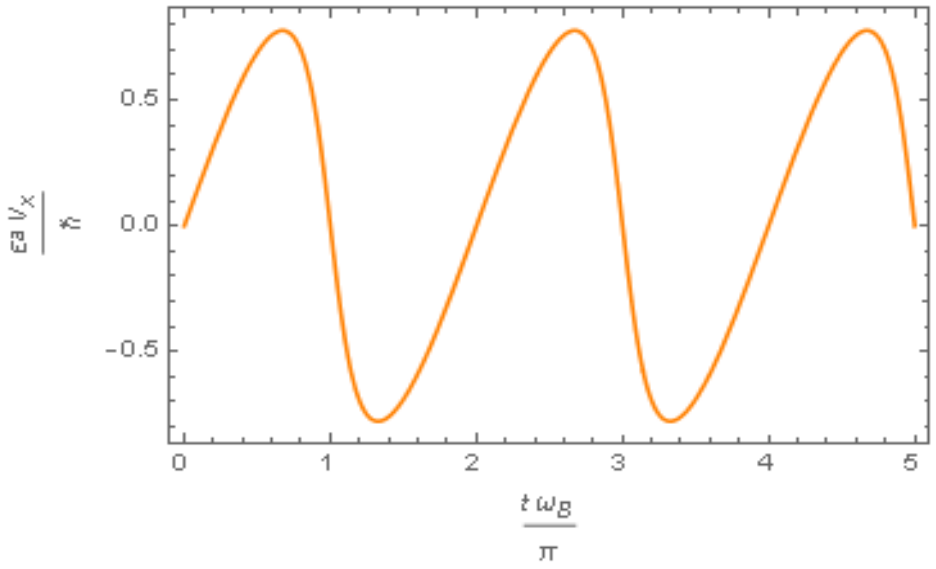

Figure 6.a shows the behavior of x-component of electron velocity $v_x(t)$ against $\frac{t\omega_B}{\pi}$ when $\frac{\sqrt{3}}{2}ak_y = \frac{\pi}{3}$. In comparison with Fig 3.3 the period of v_x and amplitude are doubled because of the electron transfer from the conduction band to the valance band and behave as a hole, so in this prosses pass through the DPs.

Figure 6.A

The electron velocity $\frac{\boldsymbol{v_x\, a\varepsilon}}{\hbar}$ *verses* $\frac{\boldsymbol{t\omega_B}}{\boldsymbol{\pi}}$ *when* $\frac{\sqrt{3}}{2}\boldsymbol{ak_y} = \frac{\boldsymbol{\pi}}{\boldsymbol{3}}$.

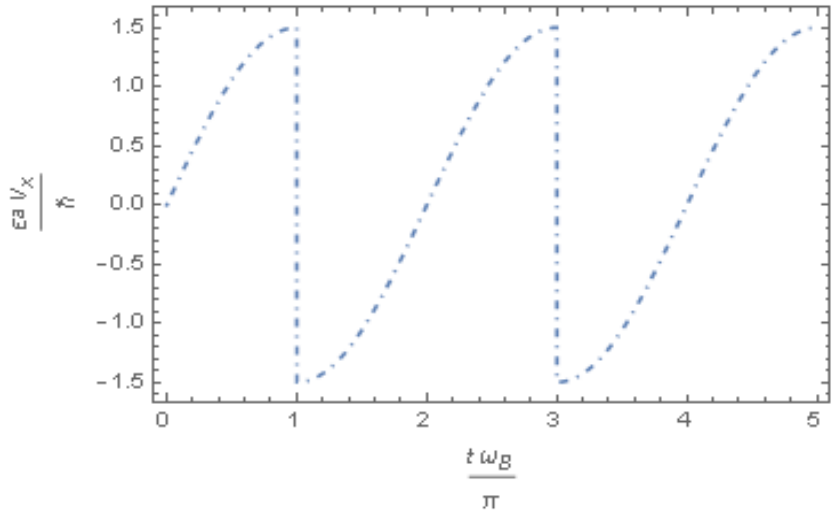

Figure 6.b shows the function of v_x against $\frac{t\omega_B}{\pi}$ when $\frac{\sqrt{3}}{2}ak_y = \frac{\pi}{4}$.

Figure 6.B

The electron velocity $\frac{v_x\, a\varepsilon}{\hbar}$ *is measured against* $\frac{t\omega_B}{\pi}$ *when* $\frac{\sqrt{3}}{2}ak_y = \frac{\pi}{4}$.

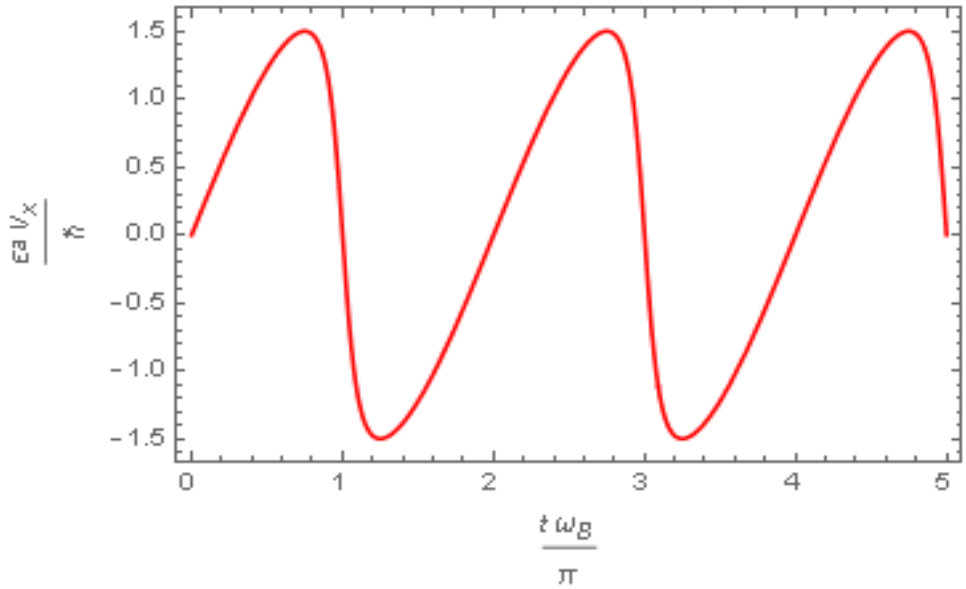

We can read the quantity on the figures in pairs (k_x, k_y). Let us take an example when $\frac{\sqrt{3}}{2}ak_y = \frac{\pi}{4}$. The first step is $E = E_x\hat{\imath}$.

$$k_x(t) = -\frac{qE_x}{\hbar}t$$

$$\omega_B = \frac{3}{2}\frac{|qaE_x|}{\hbar} = \frac{3}{2}\frac{qaE_x}{\hbar} \quad \rightarrow \quad \frac{2\omega_B}{3a} = \frac{qE_x}{\hbar}$$

So $k_x(t) = -\frac{2\omega_B}{3a}t$, then multiply by $\frac{3a}{2\pi}$:

$$\frac{3a}{2\pi}k_x(t) = -\frac{\omega_B}{\pi}t$$

when $\frac{\sqrt{3}}{2}ak_y = \frac{\pi}{4}$ $\quad \rightarrow \quad k_y = \frac{2\pi}{4\sqrt{3}}\frac{1}{a} = \frac{\pi}{2\sqrt{3}a}$

Let $\frac{\omega_B}{\pi}t = 2$ units $\rightarrow \frac{3a}{2\pi}k_x(t) = -2$

$$k_x(t) = -\frac{4\pi}{3a}$$

So, when $\frac{\sqrt{3}}{2}ak_y = \frac{\pi}{4}$, (k_x, k_y)=$(-\frac{4\pi}{3a}, \frac{\pi}{2\sqrt{3}a})$.

We can do the same for all the units in these figures. We notice that when k_x is changed $\omega_B$will change.

Figure 6.c shows the effect of the electric field in the x-direction $E_x$against the velocity v_x for all above cases of k_y.

Figure 6.C

The velocity of the electron $\frac{v_x\, a\varepsilon}{\hbar}$ *against* $\frac{t\omega_B}{\pi}$ *with different values of* $\frac{\sqrt{3}}{2}ak_y$.

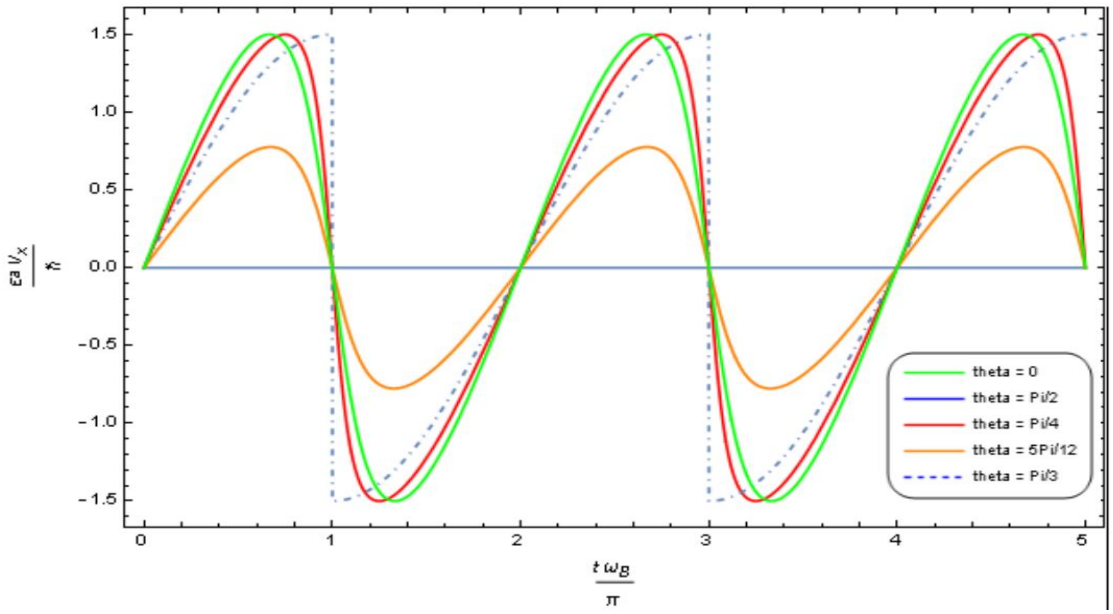

3.1.2 The velocity v_y along the y-axis:

Figure 7.a shows the effect of the electric field in the x-direction E_x on the velocity of the electron v_y against $\frac{t\omega_B}{\pi}$ when $\frac{\sqrt{3}}{2}ak_y = \frac{\pi}{2}$. There is an oscillation while $v_x = 0$.

Figure 7.A

The electron's velocity $\frac{\boldsymbol{v_y\, a\varepsilon}}{\hbar}$ *versus* $\frac{\boldsymbol{t\omega_B}}{\boldsymbol{\pi}}$ *is measured when* $\frac{\sqrt{\boldsymbol{3}}}{\boldsymbol{2}}\boldsymbol{ak_y} = \frac{\boldsymbol{\pi}}{\boldsymbol{2}}$.

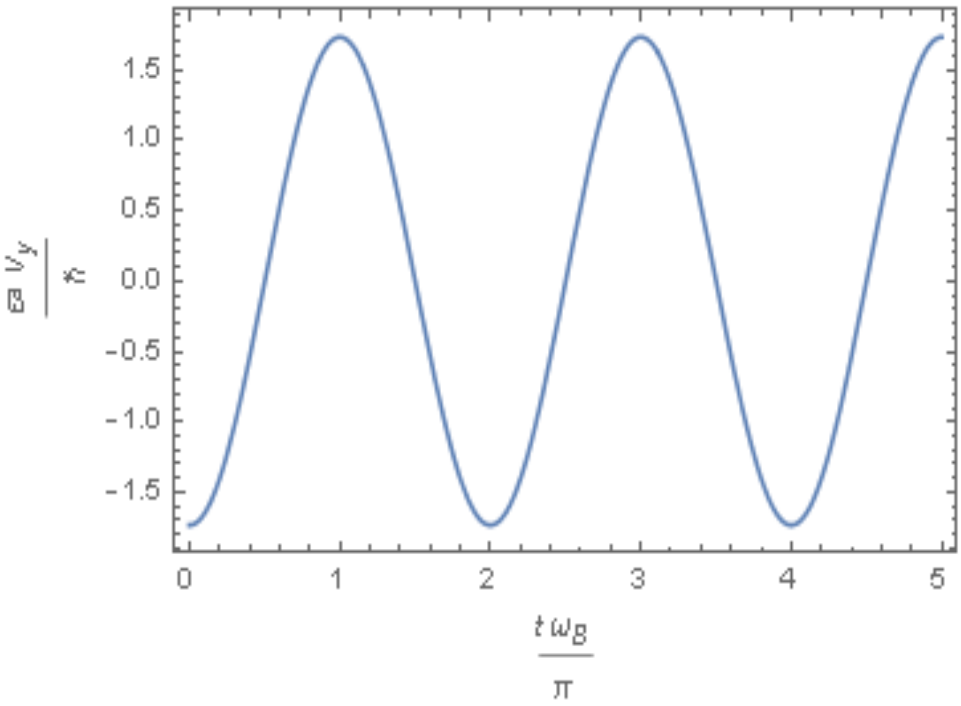

Figure 7.b shows the function of the velocity of the electron v_y against $\frac{t\omega_B}{\pi}$ when $\frac{\sqrt{3}}{2}ak_y = \frac{\pi}{4}$.

Figure 7.B

The electron velocity $\frac{v_y\, a\varepsilon}{\hbar}$ *opposes* $\frac{t\omega_B}{\pi}$ *when* $\frac{\sqrt{3}}{2}ak_y = \frac{\pi}{4}$

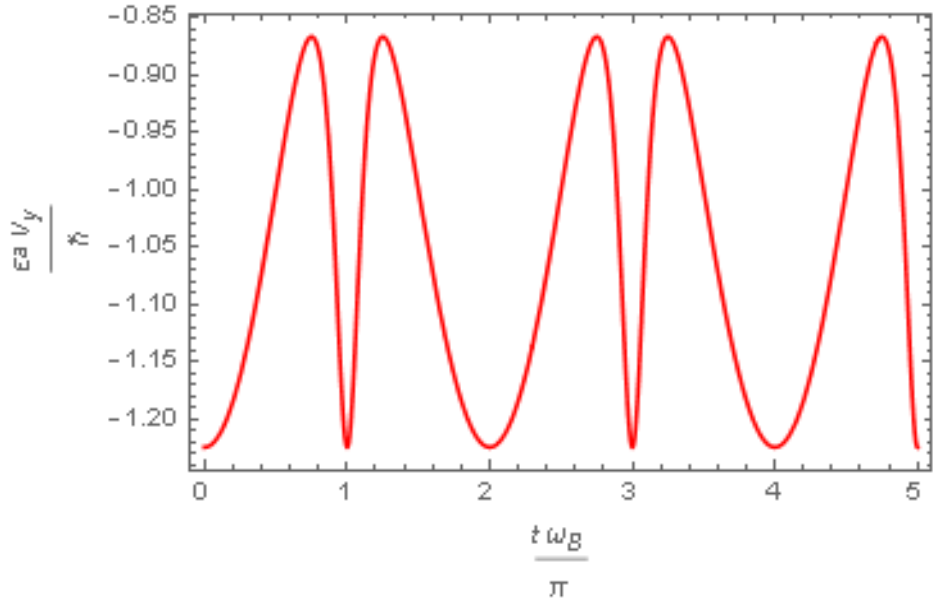

Figure 7.c shows the effect of the electric field in the x-direction $E_x$against the velocity of the electron $v_y$when $\frac{\sqrt{3}}{2}ak_y = 0$. There is no oscillation when $\frac{\sqrt{3}}{2}ak_y = n\pi$ while $v_x \neq 0$.

Figure 7.C

The velocity of the electron $\frac{v_y\, a\varepsilon}{\hbar}$ *over* $\frac{t\omega_B}{\pi}$ *when* $\frac{\sqrt{3}}{2}ak_y = 0$.

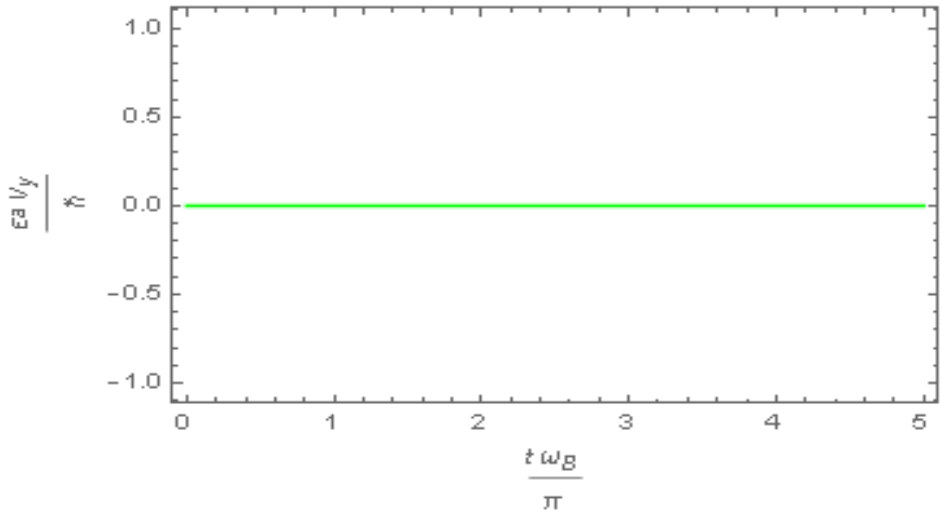

Figure 8.a shows the effect of the electric field in the x-direction $E_x$against the velocity of the electron v_yWhen $\frac{\sqrt{3}}{2}ak_y = \frac{\pi}{3}$. Compared to Fig 3.8 the period of v_y and amplitude are doubled because of the electron transfer from the conduction band to the valance band and behave as a hole, so in this prosses pass through the DPs.

Figure 8.A

The velocity of the electron $\frac{v_y\, a\varepsilon}{\hbar}$ *against* $\frac{t\omega_B}{\pi}$ *when* $\frac{\sqrt{3}}{2}\boldsymbol{ak_y} = \frac{\pi}{3}$.

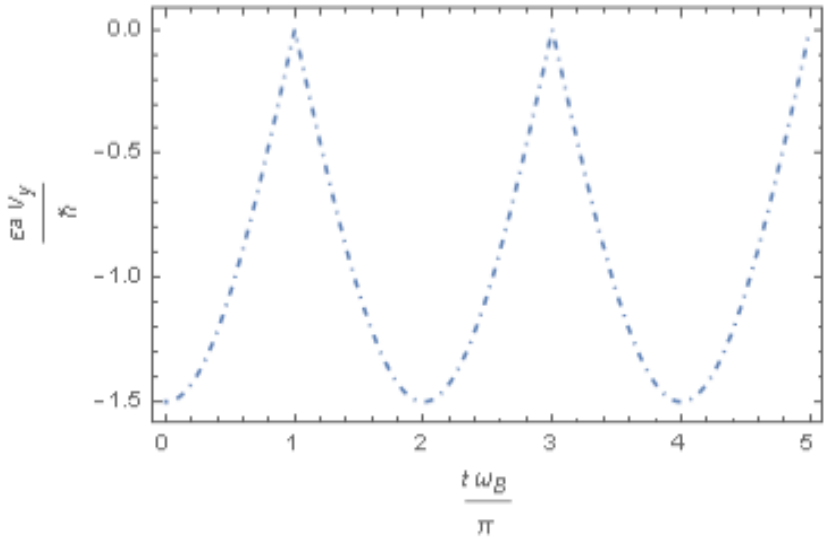

Figure 8.b shows the function of the velocity of the electron v_y versus $\frac{t\omega_B}{\pi}$when $\frac{\sqrt{3}}{2}ak_y = \frac{5\pi}{12}$.

Figure 8.B

the velocity of the electron $\frac{\boldsymbol{v_y\, a\varepsilon}}{\hbar}$ *against* $\frac{\boldsymbol{t\omega_B}}{\boldsymbol{\pi}}$ *when* $\frac{\sqrt{3}}{2}\boldsymbol{ak_y} = \frac{\boldsymbol{5\pi}}{\boldsymbol{12}}$.

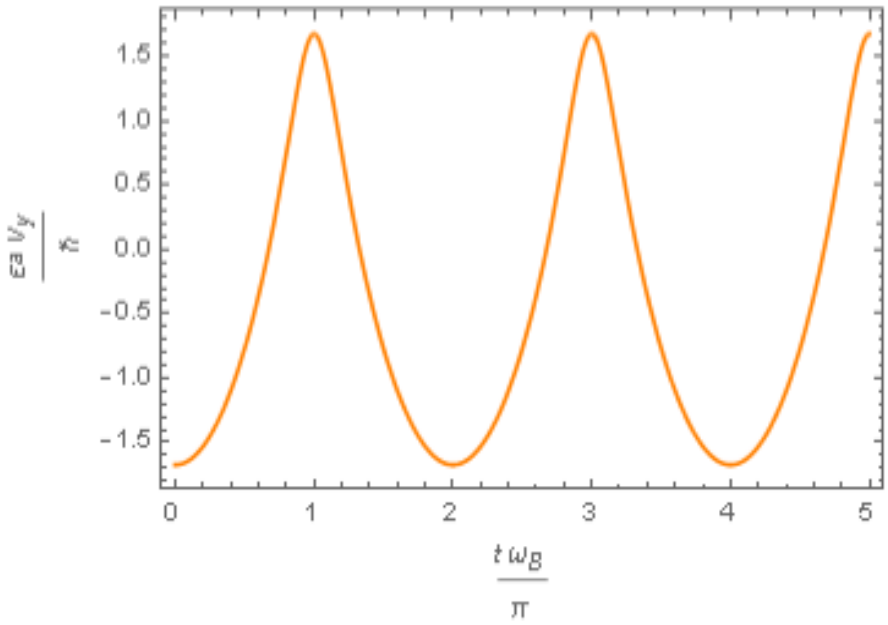

We can read the quantity on the figures in pairs (k_x, k_y) the same as the above.

3.1.3 The position of the electron under E_x:

Figure 9.a shows the effect of the electric field $E_x$on the positions $(x(t)\,, y(t)\,)$ -curve of the electron in the graphene layer when $\frac{\sqrt{3}}{2}ak_y = \frac{5\pi}{12}$. The behavior is roughly a helix so the motion will be oscillating.

Figure 9.A

The motion of the electron when $\frac{\sqrt{3}}{2}\boldsymbol{ak_y} = \frac{5\pi}{12}$.

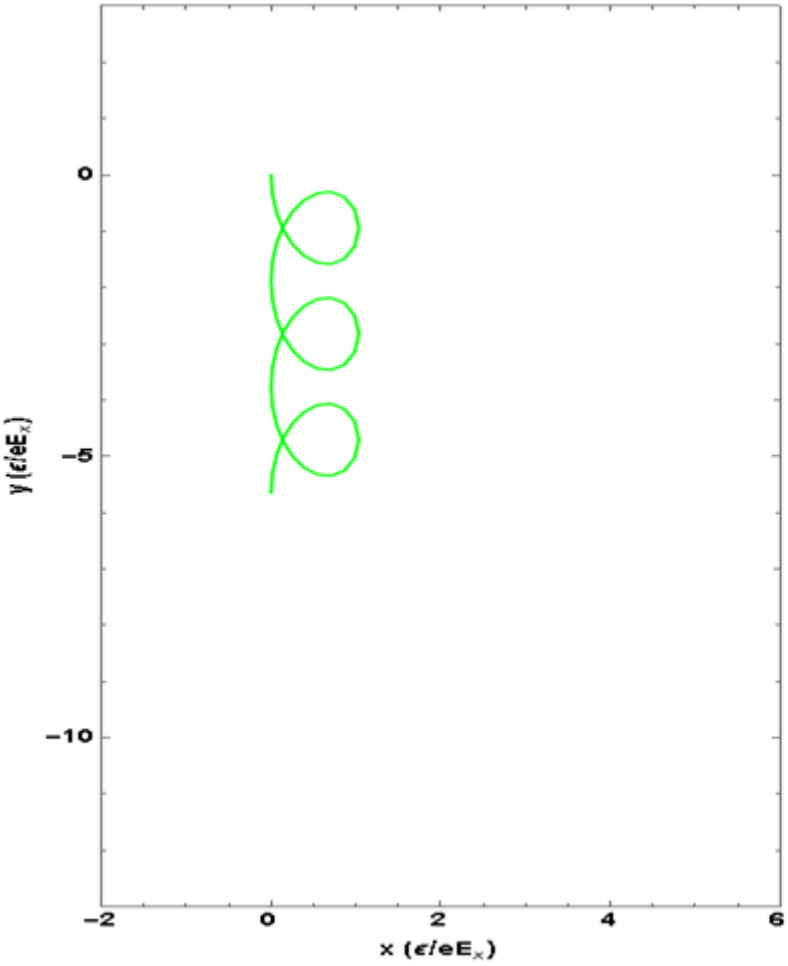

Figure 9.b shows the effect of the electric field $E_x$on the motion of the electron in the graphene layer when $\frac{\sqrt{3}}{2}ak_y = \frac{\pi}{4}$. The behavior is roughly a sine function.

Figure 9.B

The movement of the electron when $\frac{\sqrt{3}}{2}\boldsymbol{ak_y} = \frac{\pi}{4}$ *is reached.*

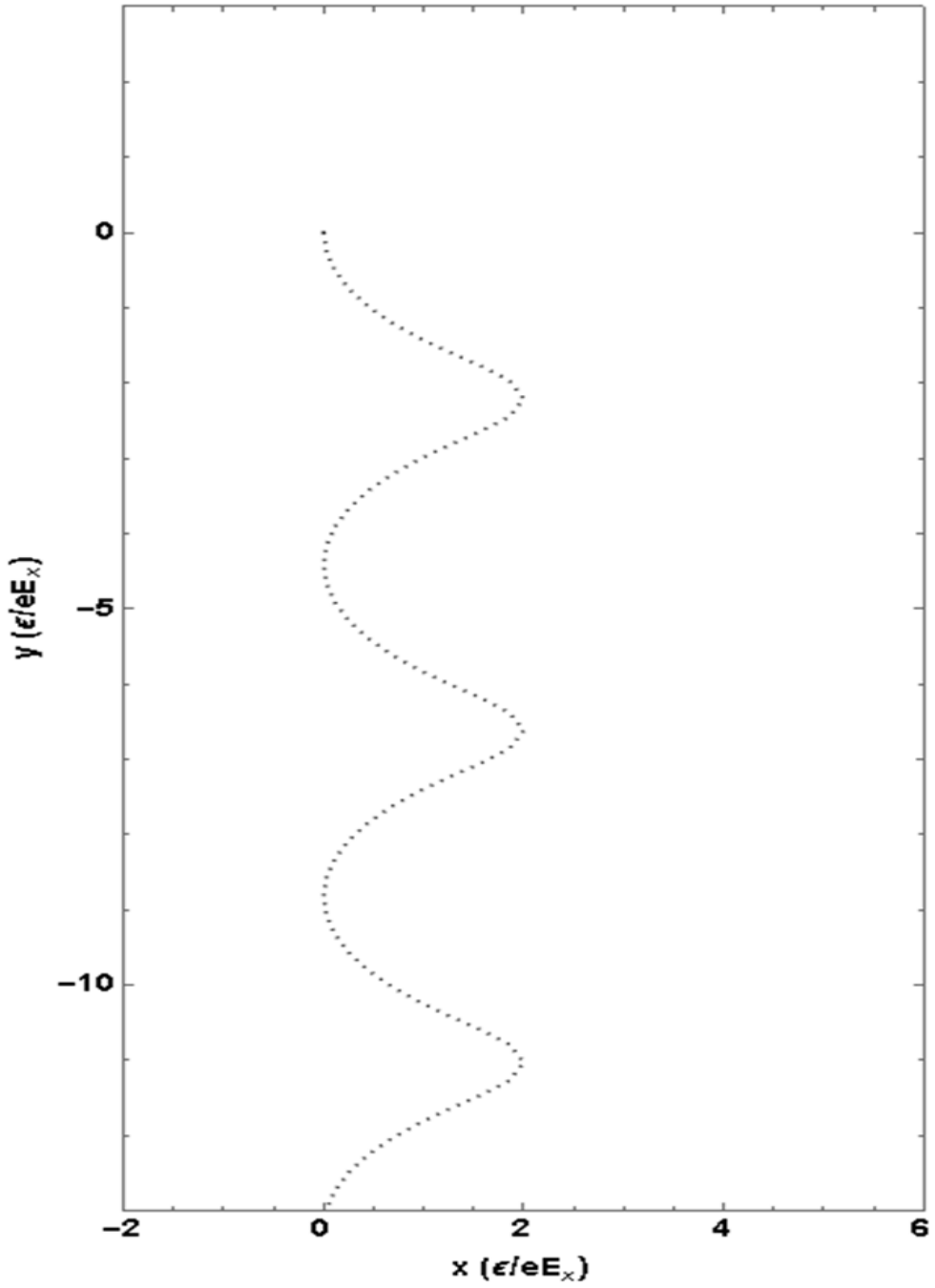

Figure 9.c shows the effect of the electric field $E_x$on the motion of the electron in the graphene layer when $\frac{\sqrt{3}}{2}ak_y = \frac{\pi}{3}$. The behavior is roughly a circle and the amplitude is doubled because the hole or electron travels through the DPs.

Figure 9.C

The electron's movement for $\frac{\sqrt{3}}{2}\boldsymbol{ak_y} = \frac{\boldsymbol{\pi}}{\boldsymbol{3}}$.

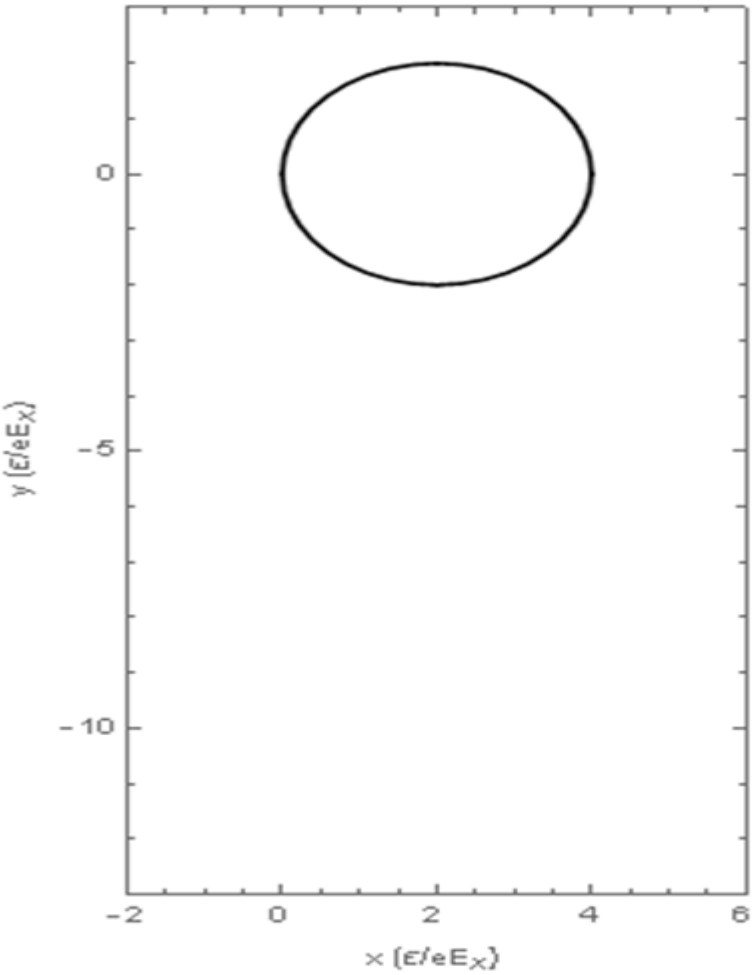

Figure 10.a shows the effect of the electric field $E_x$on the motion of the electron in the graphene layer when $\frac{\sqrt{3}}{2}ak_y = \frac{\pi}{2}$.

Figure 10.A

The motion of the electron when $\frac{\sqrt{3}}{2}\boldsymbol{ak_y} = \frac{\boldsymbol{\pi}}{\boldsymbol{2}}$.

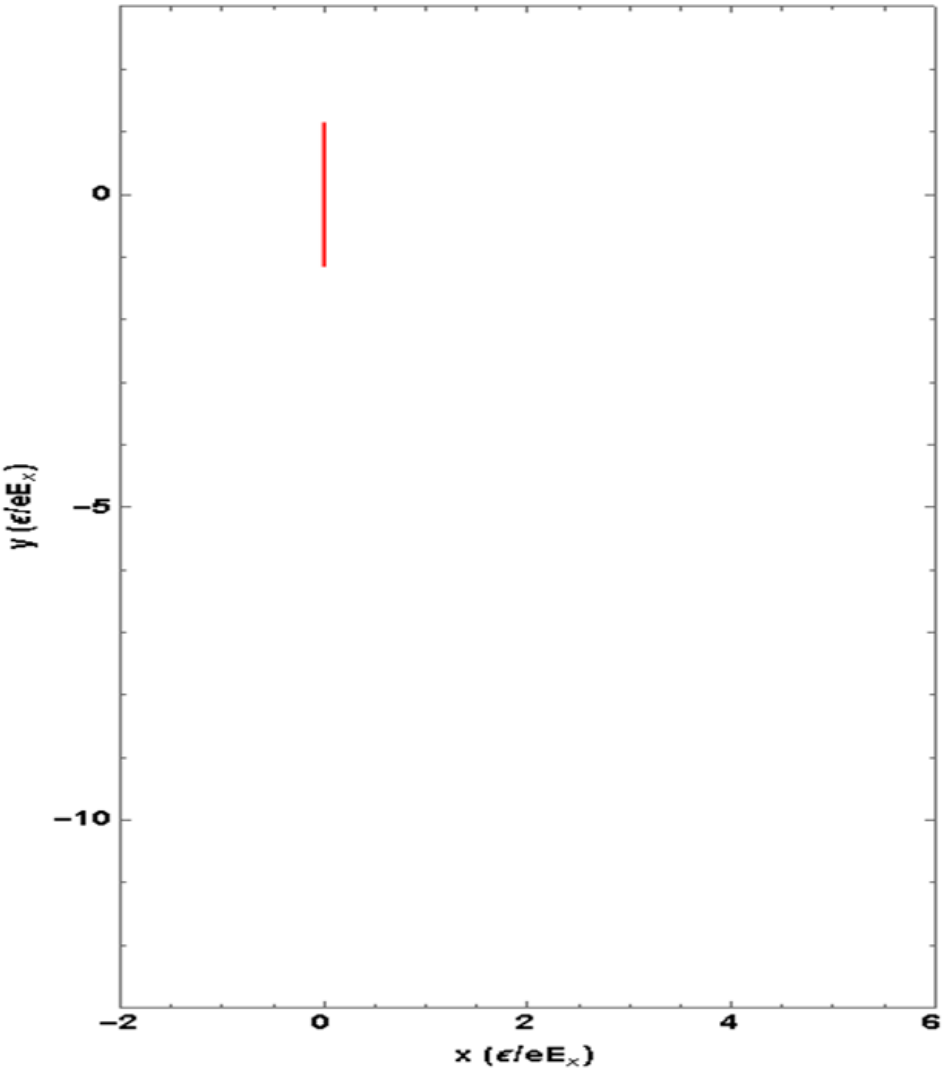

Figure 10.b shows the effect of the electric field $E_x$on the motion of the electron in the graphene layer when $\frac{\sqrt{3}}{2}ak_y = 0$.

Figure 10.B

The motion of the electron when $\frac{\sqrt{3}}{2}\boldsymbol{ak_y} = \mathbf{0}$.

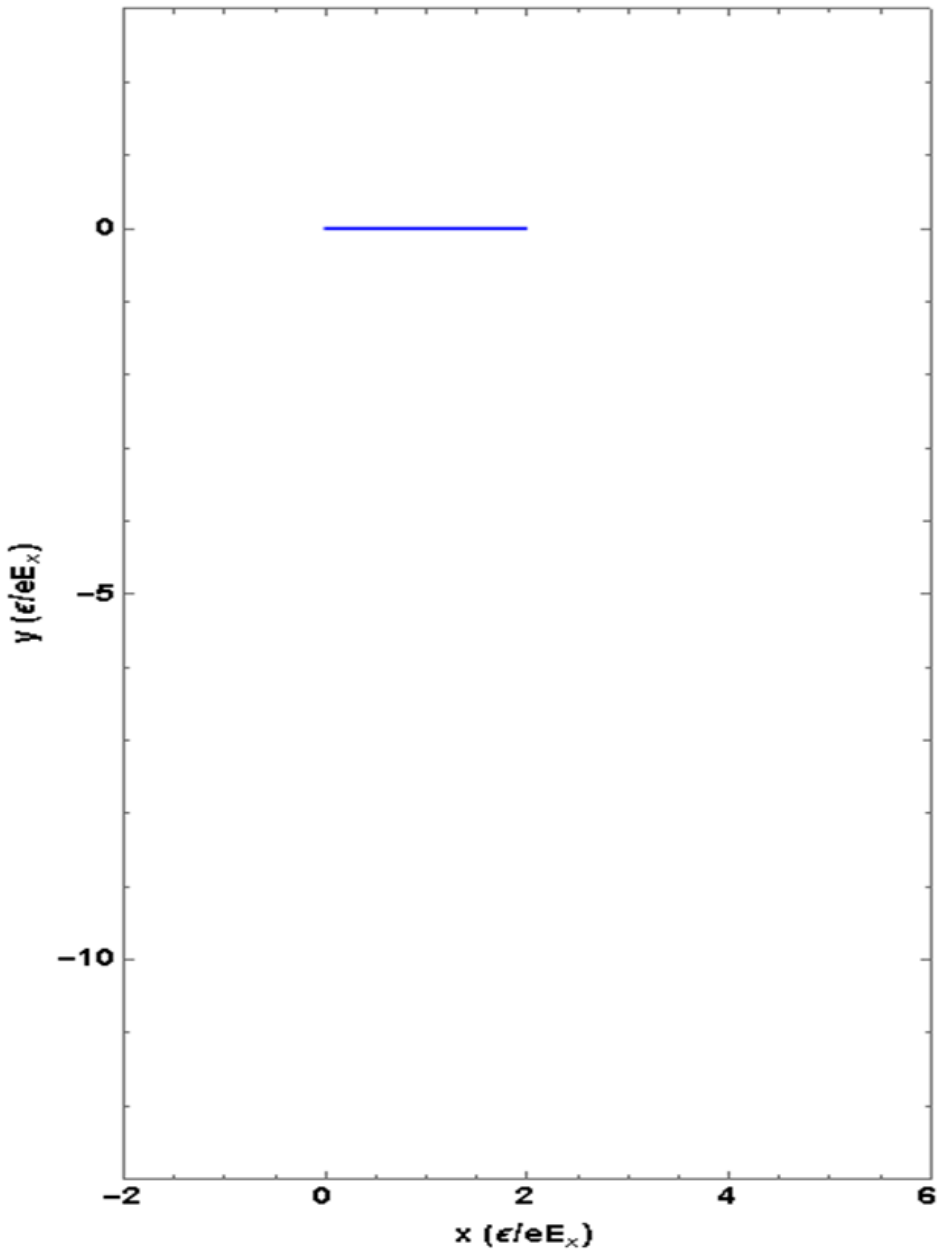

Figure 10. c shows the effect of the electric field in the x-direction $E_x$on the motion of the electron in the graphene sheet for all above cases of k_y.

Figure 10. C

The motion of the electron under the effect of $\boldsymbol{E_x}$.

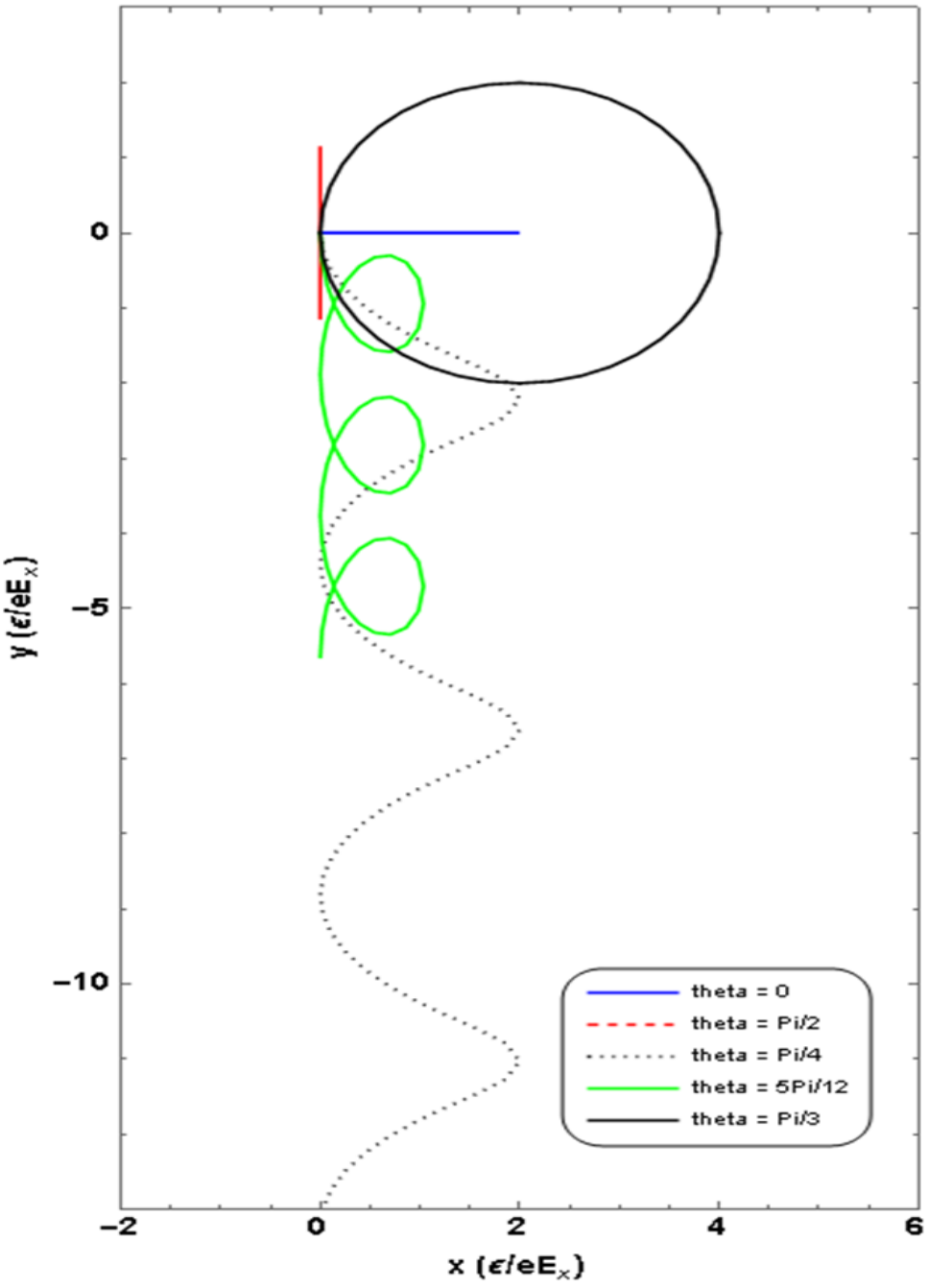

3.2 The dynamics of the electron when $\vec{E}$ along the y direction

The dynamics of the electron can be studied as the previous case. Along the y direction the oscillation amplitude L_y is:

$$L_y = |y_{max} - y_{min}| = \frac{\varepsilon}{|q\,E_y|}\left|\sqrt{4\cos\left(\frac{3}{2}k_x a\right)+5} - \sqrt{sin^2(\frac{3}{2}k_x a)}\right| \qquad (3.4)$$

When $\cos\left(\frac{3}{2}k_x a\right) = \pm 1 \quad \rightarrow \quad L_y^{max} = \frac{3\varepsilon}{|q\,E_y|}$.

When $\cos\left(\frac{3}{2}k_x a\right) = 0 \quad \rightarrow \quad L_y^{min} = \frac{(\sqrt{5}-1)\varepsilon}{|q\,E_y|}$.

In contrast to case 1, when an electric field is in the y direction, the oscillation never disappears and its amplitude never reaches zero. There is a specific condition where we notice that $v_x = 0$ when $k_x = 0$. The oscillation in the x-direction may disappear in this situation.

3.3 The dynamics of the electron when $\vec{E}$ along the x and y direction

The periods of $v_x(t)$and $v_y(t)$ becoming periodic or not periodic. However, if $\frac{T_x}{T_y}$ is irrotational, $v_x(t)$and $v_y(t)$ are not periodic and they are not limited in time. While the particle may still oscillate backward and forth through this case, the motion is not a periodic oscillation. As a result, in the obvious direction of the electric field, regular Bloch oscillations combine.

In this case the dynamics of the electron will depend on an angle α, where

$\alpha = tan^{-1}\frac{E_y}{E_x}$.

3.4 Conclusion

In this work, the graphene electron velocity has been reproduced and analyzed the dynamics of the electron under an applied electric field. We have considered the $\vec{E}$ along x and y directions. In the plane of the graphene the oscillation Bloch phenomena for the electron was studied.

The effect of the electric field is displayed in the figures between the velocity of the electron $\frac{v_y\,a\varepsilon}{\hbar}$ against the time by changing the frequency w_B. The electric field is implicitly related to electron momentum $k_x$and k_y, so we control them as $\vec{E}$ is changed.

We observed that as the electric field $\vec{E}$ is applied, the electron in a specific direction for example along x direction, the Bloch oscillation of the electron vanishes in the x direction, but it never occurs in the y direction. The computed results show that amplitude and period are doubled because the electron moves across Dirac points.

In addition, we have investigated the effect of applied electric field $\vec{E}$ in x and y direction for an electron in a monolayer of graphene with different values of angle α.

List of Abbreviations

Abbreviation	Meaning
AFM	Atomic force microscope
SPM	Scanning probe microscopy
STM	Scanning tunneling microscope
QSE	Quantum size effect
DOS	Density of states
0 D	Zero-dimension
1 D	One dimension
2D	Two dimensions
3 D	Three dimensions
$\boldsymbol{D_f}$	Number of degrees of freedom
$\boldsymbol{D_c}$	Number of the direction of quantum confinement
$\mathbf{QW_s}$	Quantum Wells
$\mathbf{QWW_s}$	Quantum Well Wires
QD	Quantum Dot
CVD	Chemical Vapor Deposition
FET	Field effect transistor
$\mathbf{DP_s}$	Dirac points
Nm	Nanometer
M	Meter
$\boldsymbol{\varepsilon}$	Energy dispersion relation
$\boldsymbol{\varepsilon_0}$	Parameter
$\boldsymbol{\vec{E}}$	External electric field
Ev	Electronvolt (1 ev= 1.602177 × 10^{-19})
A	Carbon – carbon distance (a ≈ 1.42A°)
$\boldsymbol{A^{\circ}}$	Angstroms
$\boldsymbol{\vec{E}_x}$	Electric field along the x-direction
$\boldsymbol{\vec{E}_y}$	Electric field along the y-direction
$\boldsymbol{\vec{v}_x}$	The x-component of velocity for the electron
$\boldsymbol{\vec{v}_y}$	The y-component of velocity for the electron
$\boldsymbol{\vec{F}_{ext}}$	External force
$\boldsymbol{\hbar}$	Planck constant ($\hbar$=1.054571× 10^{-34}Js)
q	Electron charge
$\boldsymbol{\omega_B}$	Bloch oscillation
T	Period
$\boldsymbol{k_x}$	x- component of wave vector
$\boldsymbol{k_y}$	y- component of wave vector
$\boldsymbol{v_B}$	Oscillation frequency
L	Amplitude
$\boldsymbol{L_x^{max}}$	Maximum amplitude
$\boldsymbol{L_x^{min}}$	Minimum amplitude
$\boldsymbol{x_{max}}$	Maximum position
$\boldsymbol{x_{min}}$	Minimum position
$\boldsymbol{E_g}$	Energy band gab

References

[1] Guisbiers, G., Mejía-Rosales, S., & Leonard Deepak, F., "Nanomaterial properties: size and shape dependencies," *Journal of Nanomaterials,* 2012.

[2] Okuno, T., Manago, M., Kitagawa, S., Ishida, K., Kusada, K., & Kitagawa, H, "NMR-based gap behavior related to the quantum size effect," *Physical Review B,* vol. 101, no. 12, p. 121406, 2020.

[3] Aoki, Hideo, and Mildred S. Dresselhaus, eds (. Aoki, Physics of graphene.., Springer Science & Business Media, 2013.

[4] Saleh, Tawfik A, " Nanomaterials: Classification, properties, and environmental toxicities," *Environmental Technology & Innovation,* vol. 20, p. 101067, 2020.

[5] Henini, M, Handbook of self assembled semiconductor nanostructures for novel devices in photonics and electronics., Elsevier, 2011.

[6] Rezaei, G., & Kish, S. S, "Effects of external electric and magnetic fields, hydrostatic pressure and temperature on the binding energy of a hydrogenic impurity confined in a two-dimensional quantum dot.," *Physica E: Low-dimensional Systems and Nanostructures,* vol. 45, pp. 56-60, 2012.

[7] Wallace, Philip Richard, "he band theory of graphite," *Physical review,* vol. 9, no. 71, p. 622., 1947.

[8] Choi, Wonbong, et al, "Synthesis of graphene and its applications: a review.," *Critical Reviews in Solid State and Materials Sciences ,* Vols. 35(1), , pp. 52-71., 2010.

[9] Scarselli, M., Castrucci, P., & De Crescenzi, M, " Electronic and optoelectronic nano-devices based on carbon nanotubes," *Journal of Physics: Condensed Matter,* vol. 31, no. 24, p. 313202, 2012.

[10] Katsnelson, Mikhail I, "Graphene: carbon in two dimensions.," *Materials today,* vol. 10, no. 1-2, pp. , 20-27, 2007.

[11] Nakkala, Poornakarthik, " Pulsed IV and RF characterization and modeling of AIGaN HEMTs and Graphene FETs (Doctoral dissertation," *Université de Limoges).*, 2015.

[12] Warda, M., & Badih, K, "Graphene Field Effect Transistors: A Review.," *arXiv preprint arXiv*, vol. 2010, p. 10382., 2020.

[13] Avsar, A., et al., "Colloquium: Spintronics in graphene and other two-dimensional materials.," *arXiv preprint arXiv:*, vol. 1909, p. 09188, 2020.

[14] Li, Xin, et al, " Graphene in photocatalysis: a review.," *Small, ,* vol. 12(48), pp. 6640-6696., 2016.

[15] Mina, A. N., Awadallah, A. A., Phillips, A. H., & Ahmed, R. R., "imulation of the band structure of graphene and carbon nanotube," . *In Journal of Physics: Conference Series*, vol. 343, no. 1, p. 012076, 2012.

[16] Fathi, Davood, "A review of electronic band structure of graphene and carbon nanotubes using tight binding.," *Journal of Nanotechnology, ,* vol. 471241., 2011.

[17] Vvedensky, Dimitri D, Quantum Theory of Matter - Graphene [Lecture Notes]., London: Imperial College., 2019.

[18] Mark Lundstrom, Density of States [Lecture 3]., Purdue University United States of America.: Nano HUB., 2011.

[19] Mas-Balleste, R., Gomez-Navarro, C., Gomez-Herrero, J., & Zamora, "2D materials: to graphene and beyond. Nanoscale," *The Royal Society of Chemistry 2011*, 2011.

[20] Chand, R., Tuteja, S. K., & Neethirajan, S., Graphene-Based Biosensors in Agro-Defense: Food Safety and Animal, John Wiley & Sons, 2019.

[21] Bhuyan, M. S. A., Uddin, M. N., Islam, M. M., Bipasha, F. A., & Hossain, S. S. , "Synthesis of graphene," *International Nano Letters,* vol. 6(2), pp. 65-83., (2016).

[22] Wei, J., Vo, T., & Inam, F, "Epoxy/graphene nanocomposites–processing and properties: a review," *Rsc Advances,* vol. 5(90), pp. 73510-73524., 2015.

[23] Nguyen, B. H., & Nguyen, V. H., "Promising applications of graphene and graphene-based nanostructures.," *Advances in Natural Sciences: Nanoscience and Nanotechnology,* Vols. , 7(2), 023002., 2016.

[24] Olabi, A. G., Abdelkareem, M. A., Wilberforce, T., & Sayed, E. T., "Application of graphene in energy storage device–A review.," *Renewable and Sustainable Energy Reviews,* Vols. 135, 110026, 2021.

[25] Novoselov KS, Geim AK, Morozov SV, Jiang D, Zhang Y, Dubonos SV, Grigorieva IV, Firsov AA, "Electric field effect in atomically thin carbon films," . *Science 306,* vol. (5696):666–669., 2004.

[26] Lukose, V., Shankar, R., & Baskaran, G., "Novel electric field effects on landau levels in graphene.," *Physical review letters,* Vols. , 98(11), 116802., 2007.

[27] Lei Liao, Xiangfeng Duan, "Graphene–dielectric integration for graphene transistors.," *Mat Sci Eng R Rep,* vol. 70(3–6):354–370., 2010.

[28] Miyazaki, H., Tsukagoshi, K., Kanda, A., Otani, M., & Okada, S., "Influence of disorder on conductance in bilayer graphene under perpendicular electric field.," *Nano letters,* Vols. , 10(10), 3888-3892., 2010.

[29] Kumar, S. B., & Guo, J. , "Multilayer graphene under vertical electric field.," *Applied Physics Letters,* Vols. , 98(22), 222101., 2011.

[30] Orozco, F. A. S., Ochoa, J. G. A., Rivas, X. C., Figueroa, J. L. C., & Carrada, H. M. M. , "Enhancing the energy spectrum of graphene quantum dot with external magnetic and Aharonov-Bohm flux fields.," *Heliyon,* Vols. 5(8), e02224., 2019.

[31] Tiryaki, A. A. S., The Electronic Band Structure of Graphene and Carbon Nanotubes, (Master thesis)., 2013.

[32] Shaer, A. A. , Heat Capacity of Two ElectronsQuantum Dot in an External Magnetic Field by Variational Method, p: (Master thesis)., 2015.

[33] Hijaz, MY. E, The Magnetization of the (GaAs) Double quantum dotsin a magnetic field., master thesis, 2016.

[34] Bzour, F. M., Effects of the hydrostatic pressure and temperature on the properties of the (GaAs) single quantum dot in a magnetic field, (Master thesis)., 2016.

[35] Ali, Mahmoud Majed Mahmoud, The magnetization of single GaAs quantum dot with Gaussian confinement, (Master thesis, An-Najah National University)., 2017.

[36] Mohammed Khalil Elsaid, and Eshtiaq Hijaz, " (2017). Magnetic susceptibility of coupled double GaAs quantum dot in magnetic fields," *Acta Physica Polonica* , vol. A. 131(6)., 2017.

[37] Ayham Shaer, Mohammad Elsaid, Eshtiaq Hijaz., "The heat capacity of a semiconductor quantum dot in magnetic fields.," *Nanosystems: Physics, Chemistry, Mathematics.,* Vols. 10: 530-535., 2019.

[38] Mohammad Elsaid, Ayham Shaer, Eshtiaq Hjaz, Muna Hajj Yahya., "Impurity effect on the magnetization and magnetic susceptibility of an electron confined in a quantum ring under the presence of an external magnetic field.," *Chinese Journal of Physics,* 2020.

[39] Huang, Tongyun, et al, "Electronic Bloch oscillation in a pristine monolayer graphene.," *Physics Letters A*, pp. , 382(42-43), 3086-3089, 2018.

[40] Prasanta Misra, Physics of condensed matter, Elsevier, 2012.

[41] Carolin Gold, et al., “Coherent jetting from a gate-defined channel in bilayer graphene,” Phys. Rev. Lett. 127, 046801 (2021)

جـامعـــة النجاح الوطنية

كليـــة الدراســـات العليـــا

تأثير المجال الكهربائي على طبقة واحدة من الجرافين

إعداد

سلسبيل خليل صالح

إشراف

أ.د. محمد السعيد

قدمت هذه الرسالة استكمالا لمتطلبات الحصول على درجة الماجستير في الفيزياء، من كلية الدراسات العليا، في جامعة النجاح الوطنية، نابلس– فلسطين.

2022

تأثير المجال الكهربائي على طبقة واحدة من الجرافين

اعداد

سلسبيل خليل صالح

اشراف

أ.د. محمد السعيد

الملخص

خلفية الدراسة: الجرافين عبارة عن مادة ثنائية الأبعاد تخضع لقوانين مواد النانو. ولدت نظرية الجرافين على يد العالم والاس عندما اكتشف البنية الالكترونية للجرافين. درس العديد من الباحثين خصائص الجرافين في وجود المجال الكهربائي. في هذه الأطروحة تمت دراسة التعابير الديناميكية للالكترون في طبقة الجرافين الأحادية في بعدين، في وجود مجال كهربائي ثابت وموحد. تم النظر في ثلاث اتجاهات مختلفة للمجال الكهربائي:

الحالة الأولى: عندما يكون المجال الكهربائي باتجاه محور السينات.

الحالة الثانية: عندما يكون المجال الكهربائي باتجاه محور الصادات.

الحالة الثالثة: عندما يكون المجال الكهربائي باتجاه محور السينات والصادات.

منهجية الدراسة: تم اشتقاق التعابير الديناميكية للسرعة والموضع للإلكترون في مجال كهربائي موجه من علاقة التشتت. تم رسم الأشكال في الحسابات من خلال استخدام برنامج الماثماتيكا.

النتائج: إن المجال الكهربائي يعتمد على التردد. وبالنظر الى أن المجال الكهربائي يعتمد ضمنياً على زخم الالكترون فانه يمكن التحكم بالمجال الكهربائي من خلال تغيير زخم الالكترون. علاوة على ذلك عندما

يكون المجال الكهربائي باتجاه محوري السينات والصادات معاً فان سلوك الالكترون في الطبقة الأحادية من الجرافين سوف يتأثر بزاوية مقدارها α.

الاستنتاجات: أظهرت هذه النتائج أنه إذا تم التأثير على الالكترون بمجال كهربائي في اتجاه معين على سبيل المثال باتجاه محور السينات فان تذبذبات بلوخ للالكترون تختفي باتجاه محور السينات ولا يمكن أن تحدث باتجاه محور الصادات. وعند مرور الالكترون في نقاط ديراك فان السعة والدورة تتضاعفان.

الكلمات المفتاحية: المجال الكهربائي، تذبذبات بلوخ، جرافين، الموقع، السرعة.